Geoscience Frontiers 15 (2024) 101866

Contents lists available at ScienceDirect

Geoscience Frontiers

journal homepage: www.elsevier.com/locate/gsf

Research Paper

Cretaceous magmatic arc in Hainan and the peri-South China Sea as evidenced by geochemical fingerprinting of granitoids in the region

Xiao-Yan Jiang [a,b], Yildirim Dilek [c], Xian-Hua Li [b,*]

[a] State Key Laboratory of Ore Deposit Geochemistry, Institute of Geochemistry, Chinese Academy of Sciences, Guiyang 550081, China
[b] State Key Laboratory of Lithospheric Evolution, Institute of Geology and Geophysics, Chinese Academy of Sciences, Beijing 100029, China
[c] Department of Geology and Environmental Earth Science, Miami University, Oxford, OH 45056, USA

ARTICLE INFO

Article history:
Received 25 December 2023
Revised 9 April 2024
Accepted 10 May 2024
Available online 11 May 2024
Handling Editor: M. Santosh

Keywords:
I–type granites
Cretaceous
Hainan Island
Southeast China
Magmatic arc
peri–South China Sea region

ABSTRACT

Mesozoic magmatic rocks occur widely in the South China Block and are generally interpreted as the manifestations of the subduction of the Paleo-Pacific oceanic lithosphere beneath Asia. Subduction-driven magmatism in southeast (SE) China continued from the Late Permian through the Late Cretaceous with an inferred lull between 125 Ma and 115 Ma that is known in the literature as the Cretaceous "*magmatic quiescence*". We report *in-situ* zircon U–Pb ages, Hf–O and whole-rock Sr–Nd isotopes, and whole-rock geochemistry of Cretaceous granitoids on Hainan Island and discuss their magmatic evolution within the framework of the Late Mesozoic geodynamics of SE China. We recognize two main stages of the emplacement of Cretaceous granitoids on Hainan, first around 120 Ma and then around 100–95 Ma, displaying high-K calc-alkaline, I-type geochemical affinities. Granites in both age groups are enriched in LILE and LREE, but depleted in Nb, Ta, Ba, Sr, and Eu. The 120 Ma granites have zircon $\varepsilon_{Hf}(t)$ values of –2.6 to 2.3 corresponding to Hf crustal model ages, ranging from 0.79 Ga to 1.03 Ga, and $\delta^{18}O$ values ranging from 6.9‰ to 7.7‰. Zircons from 100–95 Ma granites have $\varepsilon_{Hf}(t)$ values of –4.2 to 1.1 corresponding to Hf crustal model ages of 1.08 Ga to 1.42 Ga, and $\delta^{18}O$ values ranging from 6.7‰ to 8.4‰. Increasing $\varepsilon_{Hf}(t)$ values of the Cretaceous Hainan granites with younger crystallization ages indicate addition of more juvenile components and reworking of crustal material into their melt evolution. The $\varepsilon_{Nd}(t)$ values of the 120 Ma and 100–95 Ma granitoids range between –4.1 to –0.4 and –7.7 to –4.0, respectively. The calculated two–stage model age of the 100–95 Ma granitoids clusters between 1.25 Ga and 1.53 Ga. These isotopic data suggest that magmas of the Cretaceous granitoids were produced by partial melting of Mesoproterozoic metabasaltic rocks, which make up much of the crystalline basement of the southern Cathaysia block. The geochemical and isotopic characteristics of the Cretaceous granitoids on Hainan resemble those of magmatic arcs in the Circum–Pacific orogenic belts and identical to those of nearly coeval granitoid intrusions in the continental fragments within the South China Sea basin. We interpret these Cretaceous granitoids in the Peri–South China Sea region as the remnants of a once contiguous Late Mesozoic magmatic arc system that bounded the southern margin of the entire continental Southeast Asia. Our findings do not support the existence of an episode of magmatic quiescence in the geological record of SE China during the Aptian.

1. Introduction

The widespread occurrence of Mesozoic magmatic rocks in South China is one of the most conspicuous geological features of continental East Asia (Fig. 1) (e.g., Zhou and Li, 2000; Li and Li, 2007) and has been widely used to suggest the operation of an Andean-type active margin during the Mesozoic till the Late Cretaceous due to the subduction of the Paleo-Pacific Plate beneath the continent (e.g., Jahn et al., 1990; Charvet et al., 1994; Zhou and Li, 2000; Zhou et al., 2006; Li and Li, 2007; Li et al., 2012; Jiang and Li, 2014; Suo et al., 2019; Cui et al., 2021). Along with voluminous magmatism, structural grabens, local rift systems, and sedimentary basins developed in the South China Block because of the Mesozoic active margin tectonics (Dilek and Tang, 2021; Liu et al., 2021). However, this magmatic activity seems to have had a lull during the Aptian (125–115 Ma) that is known in the literature as the Cretaceous "magmatic quiescence" in SE China

* Corresponding author.
E-mail address: lixh@gig.ac.cn (X.-H. Li).

https://doi.org/10.1016/j.gsf.2024.101866

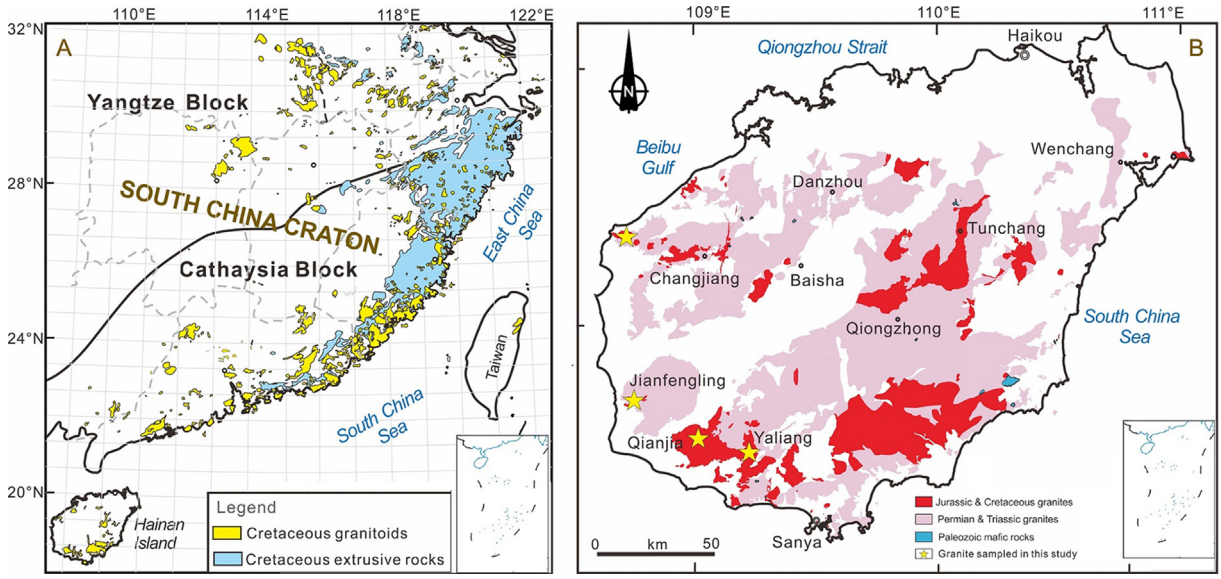

Fig. 1. Distribution of (A) Cretaceous igneous rocks in SE China (modified after Li et al., 2012), and (B) Indosinian-Yanshannian igneous rocks on Hainan Island (modified after Li et al., 2006).

(Li et al., 2010a, 2015; Mao et al., 2013; Wei et al., 2023). The cause (s) and the mode of this Early Cretaceous event are not well established.

Hainan Island is situated at the southern margin of the continental South China Block, separated from the mainland by the Qiongzhou Strait (Fig. 1). The distribution of lithological units, the structural architecture, and the regional geology of the Hainan Island reflect the geological character of the Mesozoic geology of SE China, and hence it is considered as a Mesozoic microcosm of SE China (Dilek and Tang, 2021). However, in comparison to numer-

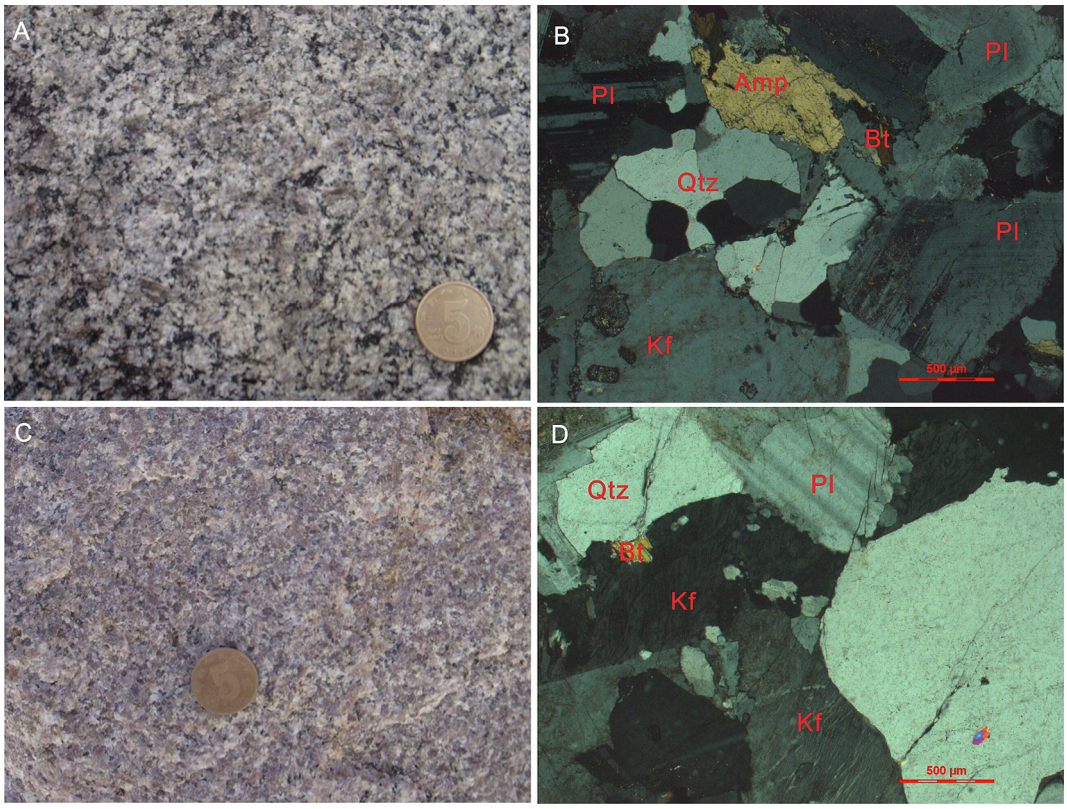

Fig. 2. Field and photomicrographs of the Cretaceous granitoid rocks on Hainan Island. (A) Field photograph of granodiorite 12HN56; (B) thin section photograph of the granodiorite sample 12HN56, showing the rock-forming minerals quartz, potassium feldspar, plagioclase, amphibole, and biotite (cross-polarized light); (C) field photograph of syenogranite sample 12HN80; (D) photomicrograph of the syenogranite sample 12HN80, showing the rock-forming minerals of quartz, potassium feldspar, plagioclase, and biotite (cross-polarized light). Mineral abbreviations: Qtz = quartz, Kfs = potassium feldspar, Pl = plagioclase, Amp = amphibole, Bt = biotite.

ous studies of magmatic rocks in the South China Block in mainland China, less attention has been paid to the Cretaceous igneous rock assemblages on Hainan Island. Consequently, the geochronological framework, and lithological and isotopic characteristics of the Cretaceous magmatic rock units on Hainan are not well documented. Previous studies have reported the occurrence of several ~ 100 Ma and ~ 73 Ma granitic plutons, and some 130–80 Ma mafic dike intrusions (Ge et al., 2003; Wang et al., 2012a; Jiang and Li, 2014; Tang et al., 2014; Zhou et al., 2015; Xu et al., 2016; Dilek and Tang, 2021).

We have investigated the Cretaceous granitoid intrusions on Hainan to: (i) document their melt sources and magmatic evolution; (ii) determine the timing of their emplacement and crystallization; (iii) present a systematic correlation of the Cretaceous magmatism and tectonic evolution of Hainan with those of the continental SE China and the adjacent continental fragments (i.e., Taiwan, Palawan, SW Borneo, SW Vietnam and S Cambodia) in the South China Sea region; and (iv) find out what the new data may tell us about the occurrence of the so-called "Cretaceous magmatic quiescence" in SE China. To this end, we undertook in-situ U-Pb and Hf-O isotope analyses of zircons from the Cretaceous granites, conducted whole-rock major and trace element geochemistry analyses of the dated samples, and obtained their Sr-Nd compositions. In the first part of the paper, we summarize the regional geology of South China and the occurrence of Cretaceous granitoids on Hainan. We then present our new geochemical, geochronological, and isotopic data on those granitoids. In the last part of the paper, we discuss the melt evolution and multi–stage development of the Cretaceous magmatism on Hainan, present a model of magmatic arc origin of this Cretaceous magmatism on Hainan and along the southern margin of continental SE China, and evaluate the validity of the Aptian "magmatic quiescence" concept in SE China. Our tectonomagmatic model has strong implications for the latest Mesozoic paleogeography of the continental margin of SE Asia and the westernmost Paleo–Pacific Ocean.

2. Regional geology background of South China Block

Separated from the North China Craton by the Qinling–Dabie Orogen to the north, the South China Block further developed when the Cathaysia block became welded into the Yangtze block during the Jiangnan orogeny in the Neoproterozoic (Charvet et al., 1996; Zhao and Cawood, 2012). The basement of the Cathaysia block contains predominantly the early Neoproterozoic volcanic and sedimentary rock successions, which were metamorphosed to greenschist–lower amphibolite facies at ~ 980 Ma. These crystalline basement rocks are overlain by the late Neoproterozoic to Paleozoic terrestrial and marine sedimentary rocks (Li et al., 2010b; Shu et al., 2011; Xia et al., 2015). The Pre-Mesozoic rocks are mainly developed to the west of the Zhenghe-Dapu Fault, generated by multiple stages of magmatism, metamorphism, and deformation at ~ 1.9–1.8 Ga, ~1.4 Ga, ~1.0–0.7 Ga, and 0.46–0.42 Ga (e.g., Li et al., 2002, 2005; Wang et al., 2012b, 2013; Shu et al., 2021). The Cathaysia block experienced extensive tectonic and magmatic events in the Mesozoic due to the subduction of the Paleo-Pacific oceanic slab beneath East Asia and acquired voluminous igneous rock suites, which can be subdivided into three groups according to their age: Permo–Triassic (~260–210 Ma), Jurassic (~190–150 Ma) and Cretaceous (~145–73 Ma) (e.g., Li and Li, 2007; Li et al., 2007, 2014a, 2020; Jiang and Li, 2014; Xu et al., 2020; Liu et al., 2021; Chen et al., 2022). The Permo–Triassic magmatism produced calc-alkaline I-type granites, peraluminous S-type granites, and minor alkaline rocks distributed in the continental hinterland and on Hainan Island that are interpreted to be the manifestations of flat-slab subduction of the Paleo–Pacific Plate or a collision between South China and other blocks (Li et al., 2006, 2012; Zhou et al., 2006; Li and Li, 2007; Wang et al., 2012b, 2013; He et al., 2020). The Jurassic igneous rocks, which are composed of I- and A-type granites and minor basaltic rocks, are mainly scattered in the Wuyishan Mountains–Nanling Range and in the adjacent regions (Zhou et al., 2006; Li et al., 2007; Guo et al., 2012a; Huang et al., 2015). Various models exist regarding their tectonomagmatic origin: foundering of a flat-slab beneath the continent (Li and Li, 2007; Li et al., 2012; Huang et al., 2015), deepening of the subduction slab angle (Zhou and Li, 2000), or intraplate rifting (Gilder et al., 1991).

Manifestations of the Late Mesozoic magmatism occur principally along the eastern and southern margins of the Cathaysia block and display a spatial pattern of oceanward (towards the SE) migration through time (Zhou et al., 2006; Zhu et al., 2014; Cao et al., 2022). The Cretaceous igneous rocks distributed along the coastal area of SE China are composed mainly of high-K calc-alkaline, I-type and subordinate A-type granites, as well as their volcanic counterparts (Fig. 1A) (Li, 2000; Zhou and Li, 2000; Zhou et al., 2006; Li and Li, 2007; Li et al., 2014b; Zhao et al., 2019; Xu et al., 2020; Chen et al., 2022). The Cretaceous granitoids in SE China comprise A- and I-type granites with minor S-type granites (Lapierre et al., 1997; Li, 2000; Zhou and Li, 2000; Zhou et al., 2006). Coeval volcanic rocks exhibit bimodal compositions dominated by > 90% felsic rocks with minor amounts (<10%) of basaltic rocks, which include the ~ 140–130 Ma Nanyuan Formation (and its equivalents) volcanic rocks and ~ 110–90 Ma Shimaoshan Group (and its equivalents) volcanic rocks (unconformably covering the foliated and metamorphosed Nanyuan Formation) (Charvet et al., 1994; Lapierre et al., 1997; Zhou et al., 2006; Guo et al., 2012b; He and Xu, 2012; Li et al., 2012, 2014a; Meng et al., 2012). In addition, Cretaceous mafic dikes locally occur within some intraplate rift basins (Li, 2000; Zhou and Li, 2000).

3. Field occurrence and mineralogy of the Cretaceous granitoids of Hainan

Located in the northwestern margin of the South China Sea (Fig. 1A), Hainan Island occurs tectonically at the intersection of the Pacific oceanic plate, the Indochina Block, and the southern margin of the South China Block (Li, 2002; Metcalfe, 2009). Because of the similarities of their geology, the Hainan Island is commonly considered as part of the Cathaysian block (Li et al., 2002, 2008). The metamorphic basement exposed on the island consists of: (i) ~ 1.43 Ga amphibolite-facies gneissic granitoids and minor metasedimentary and metavolcanic rocks of the Baoban complex; (ii) ~ 1.44–1.43 Ga greenschist-facies metasedimentary-metavolcanic rocks of the Shilu Group; and (iii) unconformably overlying ~ 1.2–1.0 Ga quartzite and quartzo-schists of the Shihuiding Formation (Li et al., 2002, 2008; Yao et al., 2017). Phanerozoic sedimentary rock sequences (except for the Devonian and Jurassic strata) and Cenozoic basalts also crop out on Hainan (Wang et al., 1991; Liu et al., 2015; Tian et al., 2021).

Granitoid intrusions are widespread on Hainan Island (Fig. 1B), accounting for ~ 40% of the island's surface area (Wang et al., 1991). Apart from the deformed Middle Permian gneissic granites at Wuzhishan in the central part of the island (Li et al., 2006), Late Permian to Triassic granitoids (ca. 270–230 Ma) are composed mainly of massive and porphyritic syenogranite, monzogranite, and granodiorite (e.g., Wang et al., 1991, 2012a; Ge, 2003; Xie et al., 2005, 2006; Li et al., 2006; Tang et al., 2013; Jiang and Li, 2014; Dilek and Tang, 2021). Subordinate Yanshanian (mainly Cretaceous) granitoid intrusions and their volcanic counterparts are recognized throughout the island. With the exceptions of several

well–dated plutons, high-precision geochronological studies of the Yanshannian granitoid rocks are yet to be done.

In this study, we have investigated a series of granitic plutons in the Yaliang, Qianjia, Jianfengling, and Changjiang areas of the island (Fig. 1B). The Yaliang and Jianfengling plutons in the south are intrusive into the Permian–Triassic granitoids and are relatively small in size. The Qianjia and Changjiang plutons are intrusive into Lower Paleozoic strata or Upper Paleozoic rock bodies in the NE and SW parts of Hainan, respectively, cover large areas, and are overlain by Quaternary deposits.

The Yaliang granodiorite in the south–central part of the island is a medium- to coarse-grained pluton, consisting mainly of euhedral to subhedral tabular plagioclase and alkaline feldspar (Fig. 2). Xenomorphic, granular quartz and minor, platy dark-green biotite also occur in these rocks, with accessory minerals of zircon and apatite.

A medium-grained porphyritic biotite-amphibole monzogranite collected from the central part of the Qianjia Pluton in the south (Fig. 1B) shows a perthitic texture in alkaline feldspar phenocrysts (~30 vol%) and contains quartz (~30 vol%) and plagioclase (~30 vol%) as the main components of the matrix. Plagioclase laths are tabular, exhibiting polysynthetic twinning. Xenomorphic granular quartz grains are interspersed with feldspar and mafic minerals (Fig. 2)). Minor minerals include biotite (~3 vol%) and amphibole (~5 vol%). Apatite, zircon, magnetite, and sphene form accessory mineral phases.

The Jiangfengling pluton in the SW part of the island is a subrounded, composite granitic intrusion (Fig. 1B). The main part of this pluton consists of Triassic massive biotite-syenogranite and monzogranite. A small exposure of a coeval diorite intrusion occurs along the outer rim of the Jiangfengling pluton. The mineral assemblage of the dioritic rock includes quartz, potassium feldspar, plagioclase, and biotite. The accessory minerals are zircon, apatite, sphene, and magnetite/ilmenite.

The Changjiang granite porphyry in the west-central part of the island occurs in the form of dikes in a pluton, which displays a typical porphyritic texture with large crystals of idiomorphic and tabular, pink K-feldspar and anhedral, granular quartz grains. Minor plagioclase, sphene and biotite are also observed in thin section. The accessory minerals include apatite, zircon, magnetite, and ilmenite.

4. Analytical methods

4.1. SIMS zircon U-Pb dating

Zircons were separated from rock samples using standard density and magnetic separation techniques. Approximately two hundred zircon grains from each sample, together with zircon standards, were loaded onto an epoxy mount. The mount was then polished to section the zircon grains in half. Zircons were imaged in transmitted and reflected-light photomicrographs, as well as in cathodoluminescence (CL) images, to reveal their internal structures. The zircon mount was then vacuum-coated with high-purity gold, prior to SIMS analysis.

Zircon U–Pb isotopes were analyzed on a Cameca 1280 SIMS at the Institute of Geology and Geophysics, Chinese Academy of Sciences (IGG–CAS), using standard operating conditions (7-scan duty cycle, ~8 nA primary O_2^- beam, 20 μm × 30 μm analytical spot size, mass resolution ~ 5400). A single electron multiplier was used in ion-counting mode to measure secondary ion beam intensities by peak jumping. U–Pb ratios were determined relative to the standard zircon Plešovice ($^{206}Pb/^{238}U$ = 0.05369, corresponding to 337.1 Ma; Sláma et al., 2008), and the absolute abundances were determined relative to the standard zircon M257 (U = 840 ppm, Th/U = 0.27; Nasdala et al., 2008). Analyses of Plešovice were interspersed with those of unknown grains, using operating and data processing procedures described by Li et al. (2009). A long-term uncertainty of 1.5% (1RSD) for $^{206}Pb/^{238}U$ measurements of the standard zircons was propagated to the unknowns (Li et al., 2010b), even though the measured $^{206}Pb/^{238}U$ error during this study is ~ 1% (1 RSD). Measured Pb isotopic compositions were corrected for common Pb, using the ^{204}Pb-method. An average Pb of present-day crustal composition (Stacey and Kramers, 1975) is used for the common Pb correction, assuming that it is largely due to surface contamination introduced during sample preparation. Uncertainties on individual analysis in the data table are reported at 1σ level; mean ages for pooled U/Pb analyses are quoted with 95% confidence intervals. Data reduction was carried out using the Isoplot/Exv. 3.70 program (Ludwig, 2008). SIMS zircon U–Pb age data are given in **Supplementary Data Table S1.**

In order to monitor the external uncertainties of SIMS U-Pb measurements, analyses of an in-house zircon standard Qinghu were interspersed with unknowns. Forty-nine analyses of this standard zircon yielded a Concordia age of 159.8 ± 0.7 Ma (MSWD of concordance = 0.16), identical within a margin of error to its reported age of 159.5 ± 0.2 Ma (Li et al., 2013).

4.2. Major and trace element analyses

Geochemical analyses of our granite samples were carried out at the Guangzhou Institute of Geochemistry, Chinese Academy of Sciences (GIG-CAS). Major element oxides were measured by a Rigaku RIX 2000 X-ray fluorescence spectrometry (XRF) in the form of fused glass beads. Precision for the analytical results is typically 1%–5%. An Agilent 7500a quadruple ICP–MS (inductively coupled plasma mass spectrometry) was used for determining trace elements. The signal drift of the spectrometer was monitored by an internal standard Rh solution. Analytical uncertainties for most elements are generally < 5%. The operational and calibrated procedures for the major and trace element analyses are similar to those detailed by Li (2002). Major and trace element analyses are listed in **Supplementary Data Table S2**.

4.3. In-situ zircon Hf-O isotopic analyses

In-situ Hf-O isotope analyses were conducted on zircons with obtained crystallization ages from the dated samples. Before SIMS oxygen isotope analysis was done, the sample zircon mount was reground to ensure that any oxygen implanted in the zircon surface from the O_2^- beam used for U-Pb analysis was removed. LA-MC-ICPMS zircon Hf-isotope was analyzed following the SIMS oxygen isotope measurement. This sequence of measurements enables U-Pb age determinations and Hf-O isotopic compositions to be done on the sites shown in Fig. 3.

In-situ zircon Lu-Hf isotope analyses were carried out on a Neptune Plus MC-ICPMS equipped with a Geolas 193 nm excimer ArF laser-ablation system at the IGG-CAS. The analytical procedures and calibration methods are similar to those described by Wu et al. (2006). Lu-Hf isotopic analyses were obtained on the same zircon grains that were previously analyzed for U–Pb and O isotopes, with ablation pits of 60 μm in diameter. The ablation time was 26 s for each measurement at a repetition rate of 8 Hz at 10 J/cm^2. Measured $^{176}Hf/^{177}Hf$ ratios were normalized to $^{179}Hf/^{177}Hf$ = 0.7325. Standard zircon 91500 was analyzed along with unknowns to monitor the reproducibility of the data and the stability of the instrument, and it yielded a weighted average $^{176}Hf/^{177}Hf$ ratio of 0.282301 ± 0.000004 (2SE, n = 90) in good agreement (within errors) with the reported value of 0.282307 ± 0.000031 (2SD) (Wu et al., 2006). Zircon Hf isotope data are listed in **Supplementary Data Table S3**.

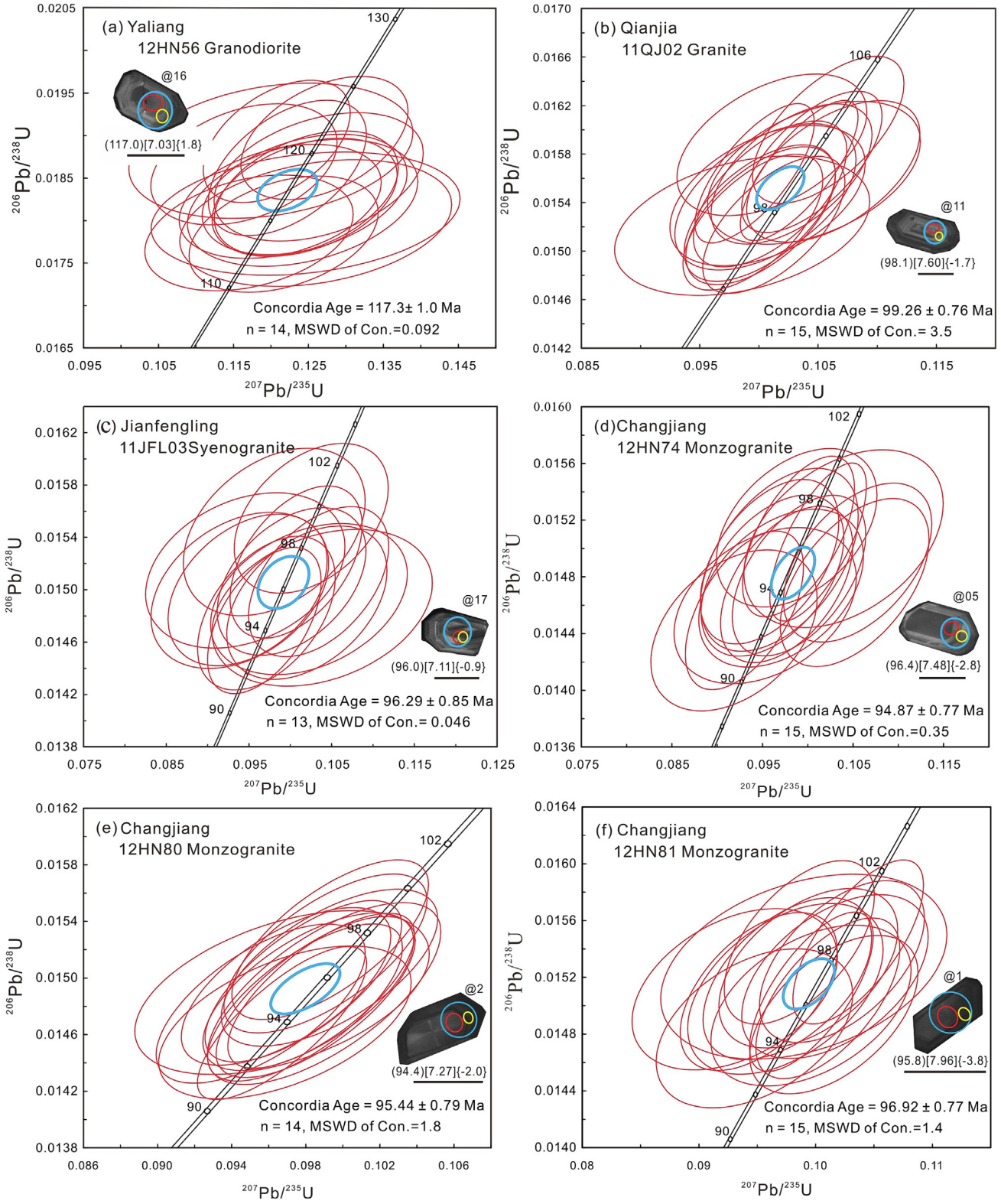

Fig. 3. SIMS U–Pb concordia age plots for zircons from the Cretaceous granitoids on Hainan Island and representative cathodoluminescence (CL) images. Photomicrographs of representative zircons analyzed for U-Pb ages, and Lu-Hf and O isotopes. Small ellipses indicate the SIMS analytical spots for U-Pb and O isotopes, and the large circles denote the LA-MC-ICP-MS analytical spots for Lu-Hf isotopes. Numbers near the analytical spots are the U-Pb ages (within parentheses), $\delta^{18}O$ values [within square brackets], and $\varepsilon_{Hf}(t)$ values {within large brackets}.

Zircon oxygen isotopes were measured using the same Cameca 1280 at SIMS laboratory in IGG-CAS. The Cs^+ ion beam was accelerated to 10 kV, with an intensity of ~ 2 nA. The analysis site was the same as for U-Pb dating, and the spot size is about 20 μm in diameter. The normal incidence electron flood gun was used to compensate for sample charging. The NMR (nuclear magnetic resonance) was used for stabilizing magnetic field. Oxygen isotopes were measured in multi-collector mode with two off-axis Faraday cups. Ana-

lytical procedures are the same way as described by Li et al. (2010c). The instrumental mass fractionation factor (IMF) was corrected using Penglai zircon standard with a $\delta^{18}O$ value of 5.31‰ (Li et al., 2010d). The internal precision of a single analysis was generally better than 0.20‰ (1σ standard error) for the $^{18}O/^{16}O$ ratio. The external precision, measured by the reproducibility of repeated analyses of Penglai standard during this study, is 0.40‰ (2SD, n = 58). During this study, an in-house zircon standard Qinghu was also measured as an unknown together with other unknowns. Twenty-seven measurements of Qinghu zircon yield a weighted mean of $\delta^{18}O$ = 5.40‰ ± 0.50‰ (2SD), which is consistent within errors with the reported value of 5.4‰ ± 0.2‰ (Li et al., 2013). Zircon O-isotope data are listed in **Supplementary Data Table S3.**

4.4. Whole-rock Sr-Nd isotopes

Chemical separation of Sr and Nd from the sample matrix was undertaken by conventional ion-exchange techniques. The detailed procedures are the same as those reported by Yang et al. (2011), and only a brief description is given here. For Sr–Nd isotopic analysis, about 100 mg of rock samples were dissolved using mixed HF + HNO_3 acid in Teflon bombs at ca. 195 °C for 2-d. Strontium and rare earth elements (REEs) were separated using AG50W × 12 (Bio-Rad) cation-exchange resin, and Nd was further separated by EICHROM © Ln-resin.

Whole-rock Sr isotopic compositions were analyzed using a Finnigan MAT 262 thermal ionization mass spectrometer at IGG-CAS. Measured $^{87}Sr/^{86}Sr$ ratios were normalized to $^{86}Sr/^{88}Sr$ = 0.1194. The replicated analyses of $^{87}Sr/^{86}Sr$ ratio of NBS SRM 987 standard solution was 0.710233 ± 0.000026 (2SD, n = 6), consistent with the recommended value of 0.710248 ± 0.000023 (Thirlwall, 1991). Whole-rock Nd isotopic measurements were performed on a Thermo Scientific Neptune MC–ICPMS at the IGG–CAS. Measured $^{143}Nd/^{144}Nd$ ratios were normalized to $^{146}Nd/^{144}Nd$ = 0.7219 using the exponential law. The measured $^{143}Nd/^{144}Nd$ ratio of the Shin Etsu JNdi-1 standard solution was 0.512108 ± 0.000014 (2SD, n = 6), consistent within errors with the recommended value of 0.512115 ± 0.000007 (Tanaka et al., 2000). The whole-rock Sr and Nd isotopic data of the studied samples are given in **Supplementary Data Table S4**.

5. Results

5.1. Zircon U-Pb ages

Zircons separated from the six granite samples are euhedral, transparent, and prismatic in crystal form, ranging in length at 30–200 μm, with aspect ratios of 1:1 to 4:1. Oscillatory zoning is common as seen in CL images (Fig. 3). The analyzed zircons have variable abundance of U (157–1720 ppm) and Th (87 – 2867 ppm) contents, with relatively high Th/U ratios (0.26–2.13), indicating their magmatic origin. Values for f_{206} are 0.00%–0.94%. All the analyses are concordant in $^{206}Pb/^{238}U$ and $^{207}Pb/^{235}Pb$ within analytical errors. Based on the results of our zircon analyses, we can separate the Cretaceous granitoid rocks into two age subgroups of 117 Ma and ca. 100–90 Ma.

The Yaliang granodiorite (12HN56) belongs to the 117 Ma subgroup. The analyses conducted on the sample yielded a Concordia age of 117.3 ± 1.0 Ma (MSWD of concordance = 0.09) (Fig. 3a) that represents the crystallization age of this granitoid. Three samples that are dated between 100 Ma and 95 Ma include granites from the Qianjia (11QJ02), Jianfengling (11JFL03), and Changjiang (12HN74, 12HN80 and 12HN81) plutons. Fifteen zircons from the Qianjia pluton gave consistent U–Pb ages of 99.3 ± 0.8 Ma (MSWD of concordance = 3.5) (Fig. 3b). Thirteen grains from the Jianfengling pluton yielded a Concordia age of 96.3 ± 0.9 Ma (MSWD of concordance = 0.046) (Fig. 3c). Analysis of 15 zircon grains from the 12HN74 (Changjiang) produced a Concordia age of 94.9 ± 1.0 Ma (MSWD of concordance = 0.35) (Fig. 3d). 12HN80 present Concordia ages of 95.4 ± 0.8 Ma (n = 15, MSWD of concordance = 1.8) (Fig. 3e). Another granite (12HN81) from Changjiang has the concordant U–Pb age 96.9 ± 0.8 Ma (n = 15, MSWD of concordance = 1.4) (Fig. 3f). The ages between 100 Ma and 95 Ma are representative of the emplacement ages of these three Cretaceous intrusive bodies.

5.2. Whole-rock geochemistry

The Cretaceous granitoid rocks exhibit a relatively wide range of chemical compositions, with SiO_2 = 65.7–77.5 wt.%, Al_2O_3 = 11.5–15.7 wt.%, CaO = 0.46–4.39 wt.%, and P_2O_5 = 0.01–0.18 wt.%. They are high in total alkalis, with K_2O = 3.59–5.10 wt.% and Na_2O = 2.79–4.09 wt.%, but low in MgO = 0.11–2.02 wt.% and $Fe_2O_3^T$ = 0.39–4.02 wt.%. On the total alkali-silica (TAS) diagram, these rocks fall into the granite and granodiorite fields, belonging to the sub-alkaline series (Fig. 4A). They are metaluminous to weakly per-

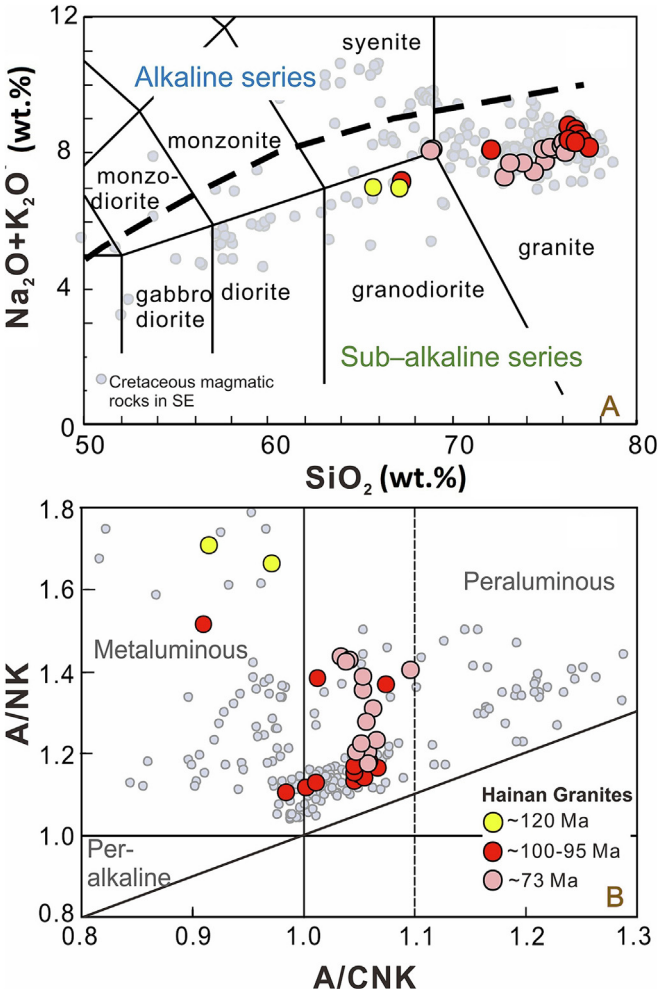

Fig. 4. (A) Rock classification diagram for the Cretaceous granitoids. (B) A/NK vs. A/CNK diagram. A/NK = Al/(Na + K) (molar ratio). A/CNK = Al/(Ca + Na + K) (molar ratio). Data for the Late Cretaceous granitoids on the Hainan Island are from Jiang and Li (2014). Data for the Cretaceous magmatic rocks in SE China are from: He et al. (2009), Jiang et al. (2011), He and Xu (2012), Chen et al. (2013, 2014a), Li et al. (2013, 2014b, 2015), Deng et al. (2014), Zhao et al. (2015).

aluminous in compositions, with A/CNK values between 0.91 and 1.07 (Fig. 4B). All samples fall into the high-K calc-alkaline series field in the SiO_2 vs. K_2O diagram (Fig. 5). According to the classification scheme of Frost et al. (2001), the samples plot in the alkali-calcic and calc-alkaline, magnesian fields (Fig. 5). The varied TiO_2, MgO, CaO, and P_2O_5 contents decrease with increasing SiO_2 contents (Fig. 5).

In the Chondrite-normalized REE diagram (Fig. 6A), the Cretaceous granitic rocks exhibit steep slopes, with the enrichment of the LREE relative to HREE, and mildly to strongly negative Eu anomalies . On the primitive mantle-normalized incompatible element spidergram (Fig. 6B), they appear enriched in LILE (e.g., Rb, Th and U) and LREE, but depleted in Nb, Ta, Ba, Sr and Eu. The zircon saturation temperatures calculated by using the equation proposed by Watson and Harrison (1983) fall between 700 °C and 800 °C.

5.3. Zircon Hf-O isotopic compositions

Zircon grains from the ca. 117 Ma granite have variable initial $^{176}Hf/^{177}Hf$ ratios ranging from 0.282632 to 0.282767, corresponding to $\varepsilon_{Hf}(t)$ of −2.6 to 2.3 (Fig. 7). The crustal Hf model age (T^C_{DM}) varies from 0.79 Ga to 1.03 Ga. Their measured $\delta^{18}O$ values range from 6.9‰ to 7.7‰ (Fig. 7). Zircon grains of the ca. 100–95 Ma granitoid rocks have variable initial $^{176}Hf/^{177}Hf$ ratios from 0.282617 to 0.282745, corresponding to $\varepsilon_{Hf}(t)$ of −4.2 to 1.1 (Fig. 7), with average crustal Hf model age (T^C_{DM}) of 1.08–1.42 Ga. In-situ oxygen isotopic analyses show relatively heterogeneous O isotopic compositions, with $\delta^{18}O_{zircon}$ values ranging from 6.7‰ to 8.4‰ (only two spots showing values > 8.0‰).

5.4. Sr-Nd isotopic compositions

Eight samples were analyzed for Sr-Nd isotopes. Both Sr and Nd isotopic compositions vary over a large range (Fig. 8). The samples from ca. 117 Ma granitic rocks have revealed $^{87}Rb/^{86}Sr$ = 0.60–1.32 and $^{87}Sr/^{86}Sr$ = 0.70689–0.70954, corresponding to initial $^{87}Sr/^{86}Sr$ ratios (I_{Sr}) = 0.7057–0.7081. Their measured $^{147}Sm/^{144}Nd$ ratios are 0.1135–0.1245 and $^{143}Nd/^{144}Nd$ ratios are 0.51237–0.51256, with calculated $\varepsilon_{Nd}(t)$ values of −0.4 to −4.1. Their calculated two-stage Nd model age (T_{2DM}) clusters around 0.94–1.24 Ga. The granitoid samples with ages of 100–95 Ma have $^{87}Rb/^{86}Sr$ ratios of 1.39–41.18 and $^{87}Sr/^{86}Sr$ ratios of 0.71020–0.78144, corresponding to more evolved and higher initial $^{87}Sr/^{86}Sr$ ratio (I_{Sr}) values of 0.7026–0.7344. However, three granitoid samples (12HN74, 12HN80 and 12HN81) have higher Rb/Sr ratios (>10), leading to higher and less reliable I_{Sr} ratios (0.7026, 0.7225 and 0.7344). Excluding those values, the obtained I_{Sr} ratios range from 0.7057 to 0.7101. The measured $^{147}Sm/^{144}Nd$ values are 0.0845–0.1204 and $^{143}Nd/^{144}Nd$ values are 0.51219–0.51239, with calculated $\varepsilon_{Nd}(t)$ values between −7.7 and −4.0. The calculated two-stage Nd model age (T_{2DM}) of these three samples clusters around 1.25–1.53 Ga.

6. Discussion

6.1. Genetic types and melt origin of the Cretaceous granitoids on Hainan

Since the introduction of the terms I- and S- type granites by Chappell and White (1974) and A-type granites by Loiselle and

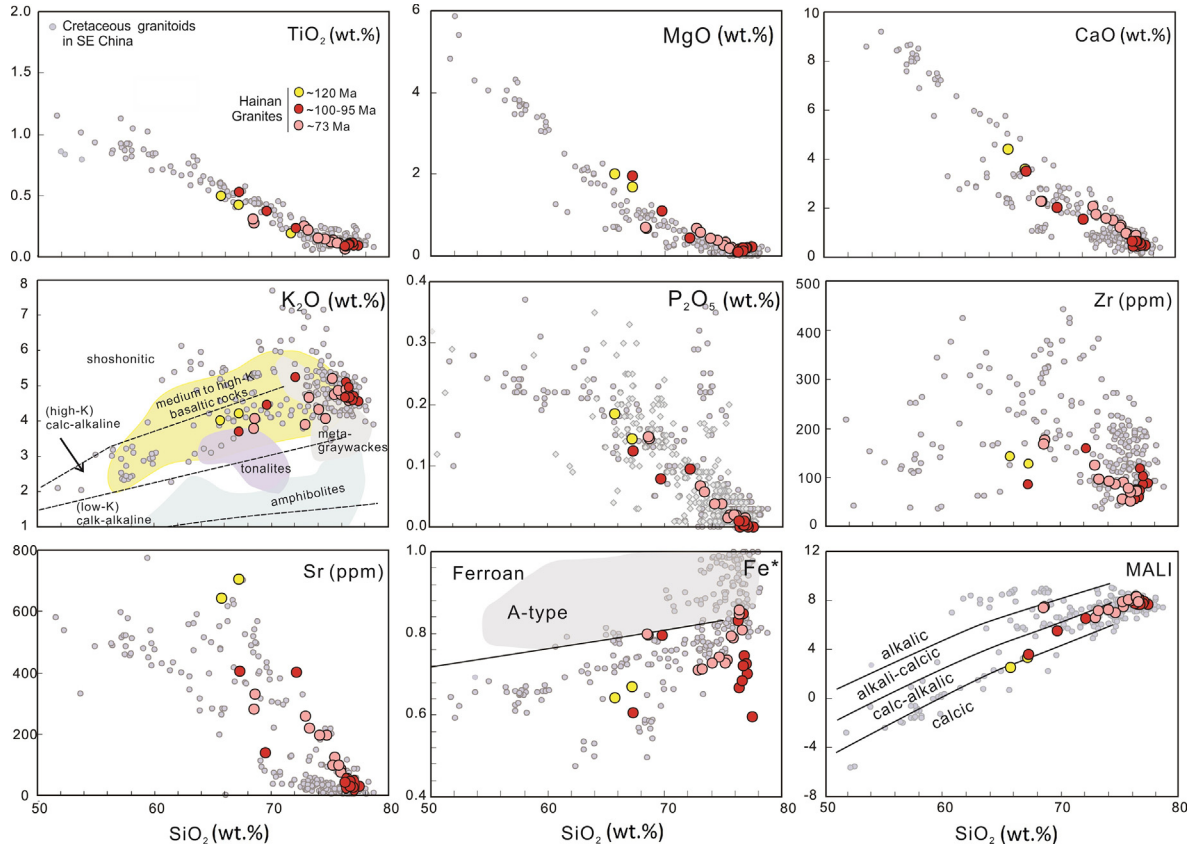

Fig. 5. Harker-type major and trace element plots for the Cretaceous granitoids. Data for the Late Cretaceous granitoids on the Hainan Island are from Jiang and Li (2014), and data for the Cretaceous intrusive rocks in SE China are from: He et al. (2009), Jiang et al. (2011), He and Xu (2012), Chen et al. (2013, 2014a), Li et al. (2013, 2014b, 2015), Deng et al. (2014), Zhao et al. (2015). Correlation between K_2O and SiO_2 contents for the Cretaceous granitoids as compared with the experimental melts by partial melting of different protoliths. Data . Sources for different protoliths: medium to high-K basaltic rocks from Sisson et al. (2005), tonalites from Singh and Johannes (1996), metagraywackes from Montel and Vielzeuf (1997), amphibolites from Rapp et al. (1991), Wolf and Wyllie (1994) and Patiño Douce (1999)

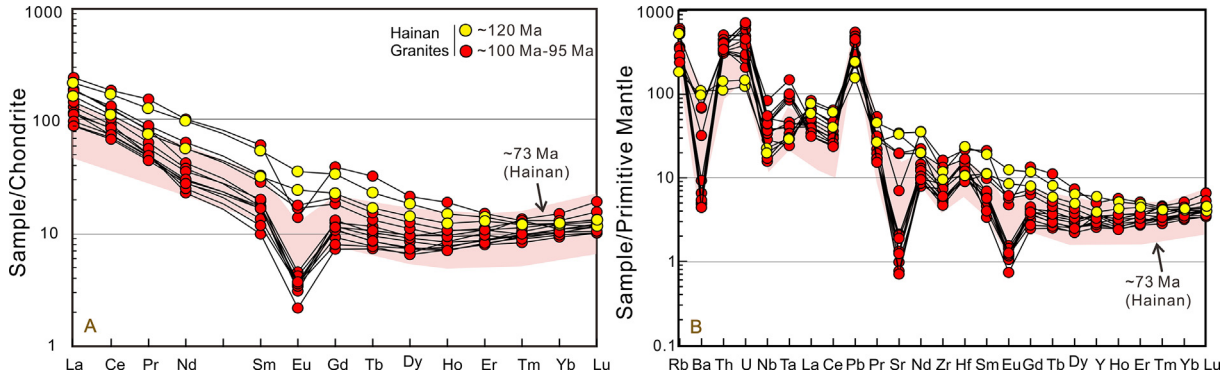

Fig. 6. (A) Chondrite-normalized REE diagram, and (B) primitive mantle-normalized trace element spidergram for the Cretaceous granitoids. Normalization values are from Sun and McDonough (1989). Data for the ca. 73 Ma granites on the Hainan Island are from Jiang and Li (2014).

Wones (1979), granites have commonly been divided into these three types according to their mineralogical and geochemical features. However, differences among these types are not always clear, especially for the case of slightly peraluminous and differentiated granites, which tend to have chemical and mineral compositions converging to those of haplogranites (e.g., Chappell and White, 2001; King et al., 2001; Chappell et al., 2004). The petrogenesis of such peraluminous, differentiated granites is commonly attributed to variable mantle–crust interactions (DePaolo, 1981; Altherr et al., 1999) or recycling of continental crystalline basement material in the melt column, followed by fractional crystallization of their magmas (Patiño Douce and McCarthy, 1998). We discuss below different parameters and variables that may have controlled the physiochemical conditions of the magmatic formation of the Cretaceous granitoids on Hainan.

The ca. 117 Ma Yaliang amphibole-bearing granodiorite samples have relatively low SiO_2 contents (<70 wt.%) and A/CNK values (0.91–0.97), and plot in the high-K calc-alkaline field (Fig. 5). All these characteristics are identical to those of typical I-type granitoids in the Lachlan Fold Belt (Chappell and White, 1992). Moreover, their relatively low $\delta^{18}O$ values (6.9‰–7.7‰) also favor an I-type affinity (Valley, 2003; Kemp et al., 2006). On the other hand, most of the ca. 100–95 Ma granites have high SiO_2 contents (>70 wt.%). The absence of alkaline minerals (riebeckite,

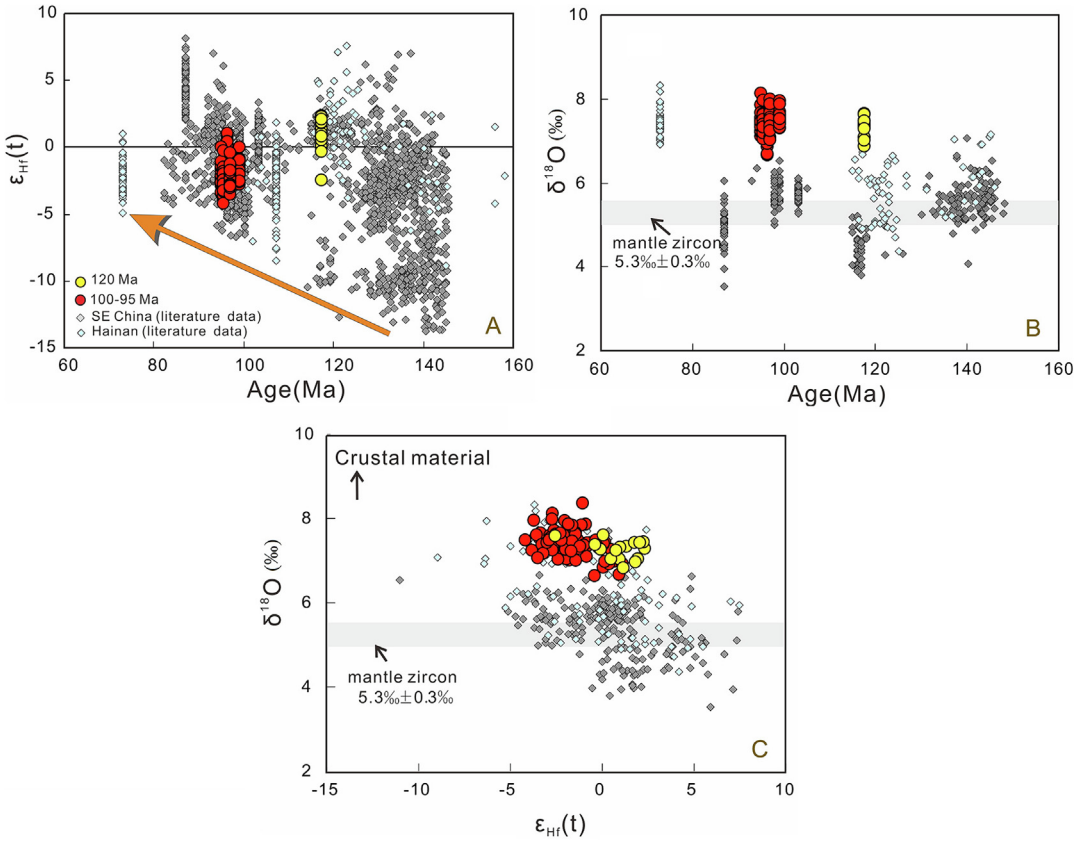

Fig. 7. (A) Crystallization ages vs. $\varepsilon_{Hf}(t)$ values of zircons with concordant ages; (B) crystallization ages versus $\delta^{18}O$ values of zircons with concordant ages; (C) $\varepsilon_{Hf}(t)$ vs. $\delta^{18}O$ values of zircons of the Cretaceous granitoids on Hainan. The Hf-isotope evolution line for Depleted Mantle and New Crust are after Griffin et al. (2000) and Dhuime et al. (2011), respectively. Mantle zircon $\delta^{18}O$ value = 5.3‰ ± 0.6‰ (2SD) (Valley et al., 1998; Page et al., 2007). Data. Sources: He et al. (2010), Guo et al. (2012b), Wang et al., (2012a), Chen et al. (2013, 2014a), Jiang and Li (2014), Liu et al. (2014), Li et al. (2015), Jiang et al. (2015).

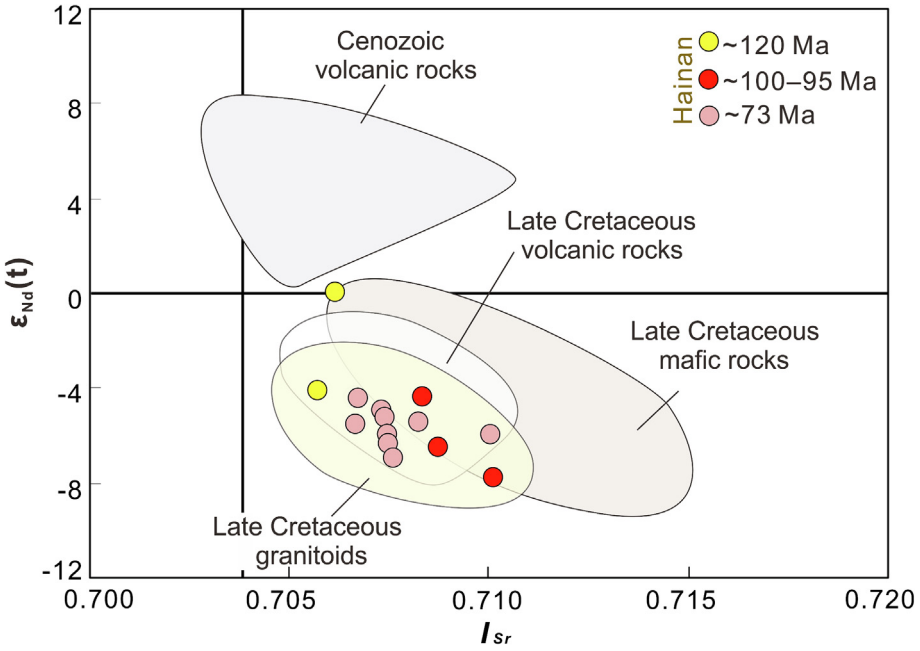

Fig. 8. Initial $^{87}Sr/^{86}Sr$ (I_{Sr}) vs. $\varepsilon_{Nd}(t)$ plot for the Cretaceous granitoids. The data of Cenozoic volcanic rocks in southeast China are from Chung et al., (1994,1995,1997), Ho et al. (2003), Zhu et al. (2004), Zhou et al. (2009), Huang et al. (2012); the data of Late Cretaceous volcanic rocks in southeast China are from Zhou and Chen (2001) and Chen et al. (2004); the data of Late Cretaceous granitoids are from Lan et al. (1995), Chen et al. (2004, 2013), Mao et al. (2006), Wang et al. (2012a); the data of Late Cretaceous mafic dikes are from Ge (2003), Qi et al.(2012), Wang et al. (2012a); the data of 73 Ma granites of Hainan Island are from Jiang and Li (2014).

arfvedsonite and aegirine) in these rocks precludes the possibility of their origin as alkaline A-type granites. Although several granodiorite samples display 10,000 × Ga/Al ratios > 2.7, the lower HFSE (Zr + Nb + Ce + Y < 330 ppm) (Fig. 9) values also exclude the possibility of their aluminous A-type origin. The observed petrological features (presence of amphibole) and geochemical characteristics (metaluminous to weakly peraluminous, and the negative correlation between SiO_2 and P_2O_5) suggest that the 100–95 Ma granitoids represent I-type granites. The $\delta^{18}O$ ratios of these granites are lower than those of the S-type granites, which are characteristically higher than 8‰ (Valley, 2003). All these features collectively indicate that these 100–95 Ma granitoids have close geochemical affinity to I-type, rather than A- or S-type granites.

Magmatic temperatures have significant implications for delineating the petrogenesis of granites. A prevalent method for the

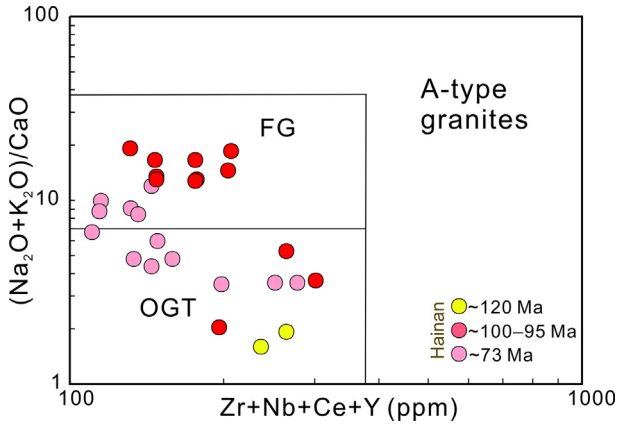

Fig. 9. Zr + Nb + Ce + Y vs. $(Na_2O + K_2O)/CaO$ diagram for the Cretaceous granitoids on the Hainan Island. Data for the Late Cretaceous granitoids on the Hainan Island are from Jiang and Li (2014).

estimation of magmatic temperatures of granites is the zircon saturation thermometer (T_{Zr}), proposed by Watson and Harrison (1983). The Cretaceous granites on Hainan show a relatively wide range of T_{Zr} between 700 °C and 800 °C. Because xenocrystal zircons are rare to absent in our rock samples and because there is a tight negative correlation between their Zr and SiO_2 values (Fig. 5), the maximum T_{Zr} temperature of each pluton provides a minimum estimate of the magmatic temperature prior to its crystallization. Therefore, the initial magmatic temperatures might have exceeded 800 °C, reminiscent of the "high temperature" and/or "hot" I-type granites (Chappell et al., 1998, 2000; Miller et al., 2003; Collins et al., 2016), which require advective heat input into the crust. Besides temperature, the oxygen fugacity is also an important factor for evaluating the physiochemical conditions of granitic magma formation (Dall'Agnol et al., 2005; Jiang et al., 2018a,b). Previous studies of the Cretaceous granites on Hainan have shown the accessory mineral assemblage of magnetite–titanite–allanite–apatite (Chen et al., 2008, 2014b), and mineralogical compositions reflecting oxidized conditions. These features are common in magmas produced in subduction–related environments (Wones, 1989).

High-K, calc-alkaline, I-type granites are generally formed by partial melting of medium- to high-K, calc-alkaline, mafic to intermediate rocks (Rapp et al., 1991; Roberts and Clemens, 1993; Rapp and Watson, 1995). Sisson et al. (2005) obtained high-K granitic melts reaching high-silica contents (SiO_2 > 65 wt.%) and Na_2O/K_2O < 1 by using medium- to high-K basaltic compositions as starting materials, similar to the compositions of those low-Si Cretaceous granites on the Hainan Island. Therefore, we consider medium- to high-K metabasaltic rocks as the best candidates for the melt source of the Cretaceous granites on Hainan (Fig. 5). Moreover, the zircon Hf isotopic compositions, which indicate their progressive change with time, suggest an increasing input of juvenile components with a younging trend (Fig. 7). Considering the two-stage Nd model and Hf model ages, we posit that magmas of the Cretaceous granites on Hainan were most likely generated by

partial melting of the regional Mesoproterozoic metabasaltic basement rocks with an input of juvenile components.

6.2. Multi-stage development of Cretaceous magmatism on Hainan and comparison with coeval magmatism in SE China

The temporal patterns of Cretaceous magmatism in mainland SE China show a nearly continuous record from 145 Ma to 80 Ma with two major peaks at ~ 130 Ma and ~ 100 Ma, and a short period of apparent quiescence from 125 Ma to 115 Ma (Fig. 10**A**; Guo et al., 2012b; He and Xu, 2012; Jiang et al., 2015, 2021; Li et al., 2015; Chen et al., 2022). Jiang and Li (2014) identified the youngest Mesozoic granite in South China as the ca. 73 Ma Longlou granite. Furthermore, Xu et al. (2016) reported three stages of magma emplacement for the origin of the Cretaceous, Mo-hosting granitoids during ca. 113–108 Ma, ca. 100–94 Ma, and ca. 90–70 Ma, respectively. Cretaceous magmatic rocks in SE China are made vastly of silicic intrusive and volcanic rock associations. Intrusive rocks are mainly gabbro, syenite, and I-type and A-type granites (Dong et al., 1997; Wong et al., 2009, 2011; He and Xu, 2012; Liu et al., 2012; Li et al., 2015a; Zhang et al., 2019; Peng et al., 2021; Chen et al., 2022).

The compilation of zircon age data reveals that magmatic rocks on Hainan Island were developed through multiple stages during the period of ca. 135–70 Ma, but mainly between 120 Ma and 90 Ma with a major peak at ca. 100 Ma (Fig. 10B). In addition to the 117 Ma Yaliang granodiorite that has been identified and described in this study for the first time, a ~ 133 Ma biotite-

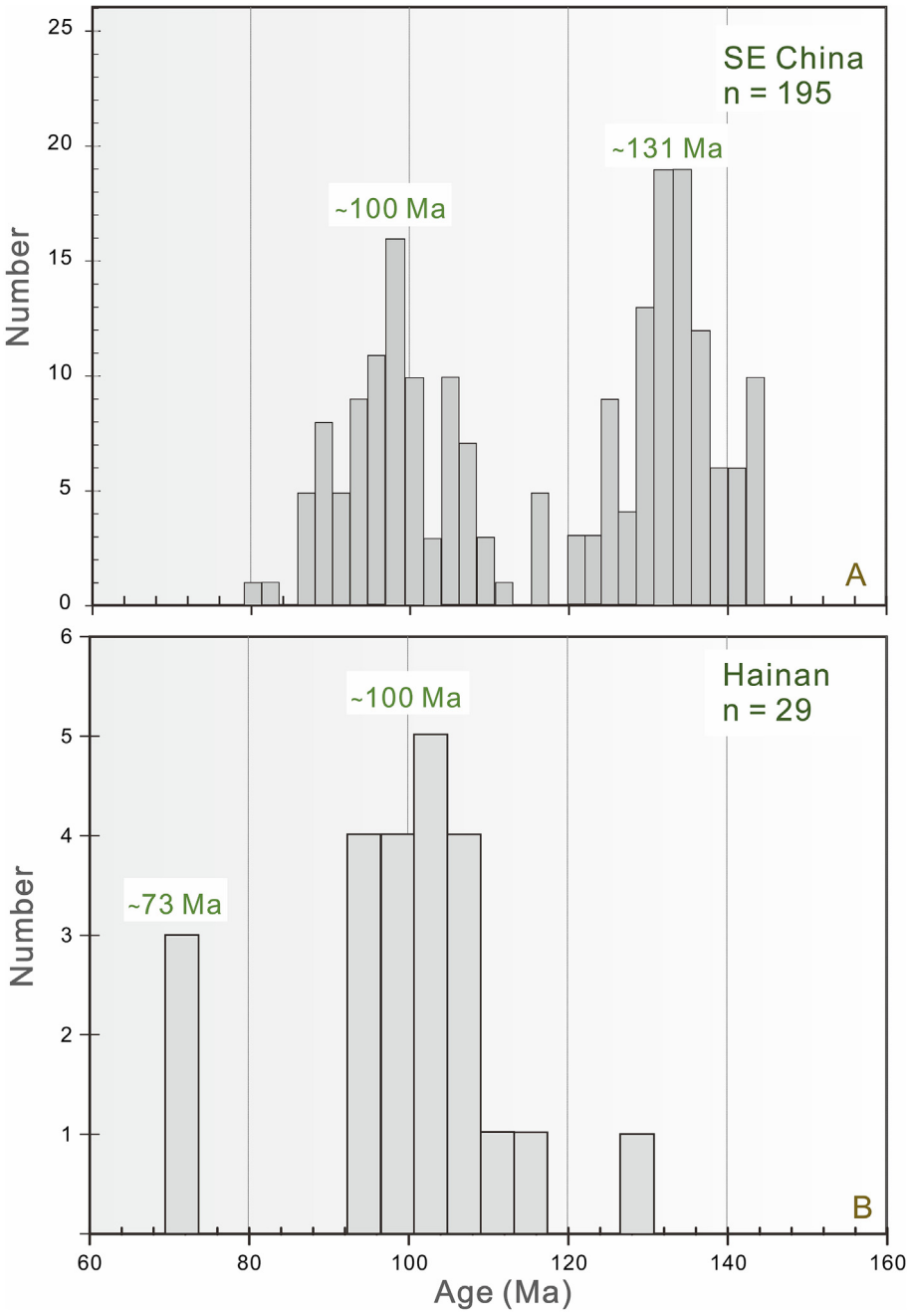

Fig. 10. Histograms and cumulative probability plots of isotopic ages for the Cretaceous igneous rocks in (A) Southeast (SE) China (Table S5), and (B) Hainan Island (Ge, 2003; Tang et al., 2010, 2013, 2014; Wang et al., 2012a; Chen et al., 2014b; Jiang and Li, 2014; Zhou et al., 2015; Li et al., 2016; Xu et al., 2016).

granite was reported in the Shilu deposit (Li et al., 2016), a 107 Ma granodiorite was found in Tunchang (Wang et al., 2012a), and some other plutons (composed of monzogranite and granodiorite) dated at ca. 107–105 Ma were discovered in the southern part of Hainan (Yan et al., 2017). All these Cretaceous plutons that formed during the 100–90 Ma time interval are distributed in the southwestern and eastern parts of the island (Chen et al., 2008; Tang et al., 2010; Wang et al., 2012a; Yan et al., 2017; Sun et al., 2018). Based on our new age data and the available geochronological information, it appears that the Cretaceous granitic magmatism on Hainan Island occurred mainly in three stages: ~135 Ma, ca. 120–90 Ma, and ca. 70 Ma.

In addition to intrusive rocks, there are also limited Cretaceous hypabyssal intrusions and volcanic rocks on the Hainan Island. Mafic dikes that are mainly distributed in the eastern and southern parts of the island are dated at ~ 135 Ma, ca. 117 Ma, ca. 105 Ma, ca. 102–90 Ma, ca. 86 Ma, and ca. 81 Ma (Ge et al., 2003; Wang et al., 2012a; Tang et al., 2014; Dilek and Tang, 2021). A suite of basalt–andesite–rhyolite volcanic rock associations has been recently identified in the southern part of the island and dated at 102 Ma (Zhou et al., 2015). Therefore, the Cretaceous hypabyssal intrusive and volcanic rocks on Hainan can be roughly divided into two broad age groups of ca.135 Ma and ca.120–80 Ma.

Compared with the temporal and lithological characteristics of the Cretaceous rock suites in mainland SE China, their counterparts on Hainan appear different. Mafic plutonic rocks are rare on Hainan and volcanic rocks are limited in exposure. The Cretaceous intrusive rocks on Hainan belong to high-K, calc-alkaline I-type granites.

6.3. Magmatic arc origin of the Cretaceous plutonic rocks on Hainan

The following observations and findings from Hainan support an extended magmatic arc origin of the Cretaceous granitoids on this island: (i) Cretaceous granitoids on Hainan (in this study and previous work) are all high-K, calc-alkaline granites, representing I-type affinities, which commonly occur in active continental margins and in continental arcs (Roberts and Clemens, 1993; Barbarin, 1999); (ii) these Cretaceous granites on Hainan are geochemically akin to granites formed in "syn-collisional" and "volcanic-arc" settings (Fig. 11), and are broadly consistent (geochemically) with the Cretaceous calc-alkaline granitic rocks in SE China; (iii) a progression of increasing $\varepsilon_{Hf}(t)$ values of granitic zircons through time in the Cretaceous (Fig. 7) suggests a systematic increase of juvenile components into the magmatic plumbing system, analogous to subduction-related magmatism in the circum–Pacific arcs and orogenic belts (Kemp et al., 2009; Collins et al., 2011); and, (iv) the geochemistry of nearly 81 Ma mafic dike swarms in southern Hainan resembles that of magmas formed by partial melting of subduction–metasomatized mantle sources in extensional tectonic settings (Ge et al., 2003).

The widespread occurrence of Cretaceous magmatic rocks, structural domes and basins, metamorphic core complexes, and sedimentary basins in SE China represent the manifestations of extensional deformation in a backarc setting above the subducting Paleo-Pacific slab and inland from this inferred magmatic arc (Li and Li, 2007; Li et al., 2014a, 2020; Zhao et al., 2017; Chu et al., 2019; Dilek and Tang, 2021). The development of the magmatic arc must have followed the trench migration and the slab retreat into the Paleo-Pacific Ocean realm to the E–SE. The ~ 100 Ma basalt, andesite, and rhyolite volcanic rock suites in SE China represent the results of subduction-related magmatism in the backarc environment behind the magmatic arc (Zhou et al., 2015).

6.4. Regional extent of the Cretaceous magmatic arc

Granitic plutonic rock associations with ages and compositions similar to those in Hainan and SE China and coeval volcanic rocks have been also reported from farther south in Southeast Asia, including the islands of Palawan and Borneo bounding the southernmost part of the South China Sea, in the Pearl River and the

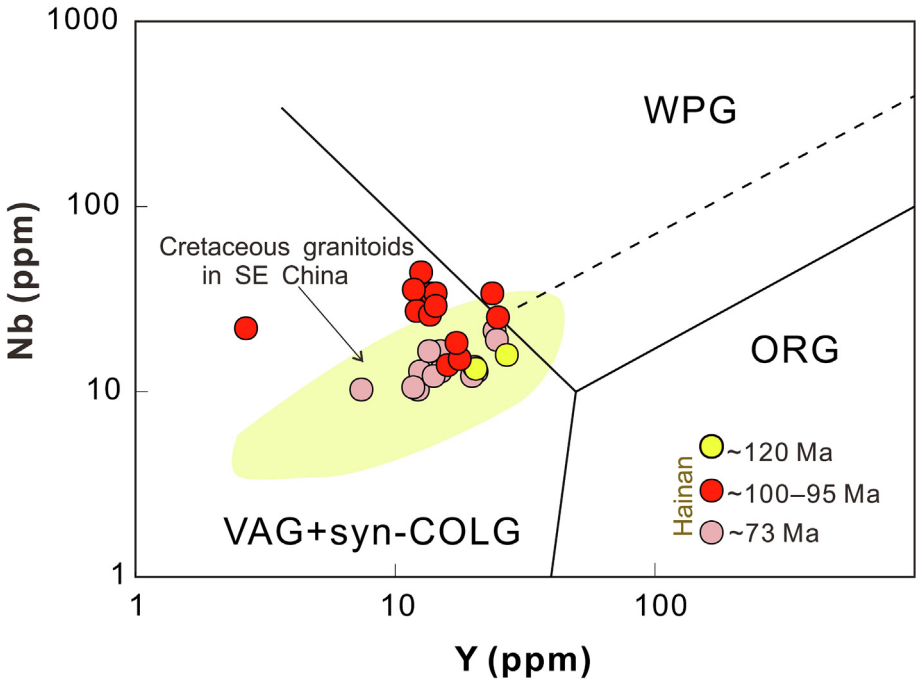

Fig. 11. Tectonic discrimination diagram (Pearce et al., 1984) for the Cretaceous granitoids that plot in the field of VAG (volcanic arc granites) and syn-COLG (syn-collisional granites). Data for the Cretaceous granitic rocks in southeast China are from Chen et al. (2004, 2013), Lan et al. (1995), Li (2000), Qiu et al. (2008) and Xing et al. (2009). Data for the Late Cretaceous granitoids on Hainan Island are from Jiang and Li (2014).

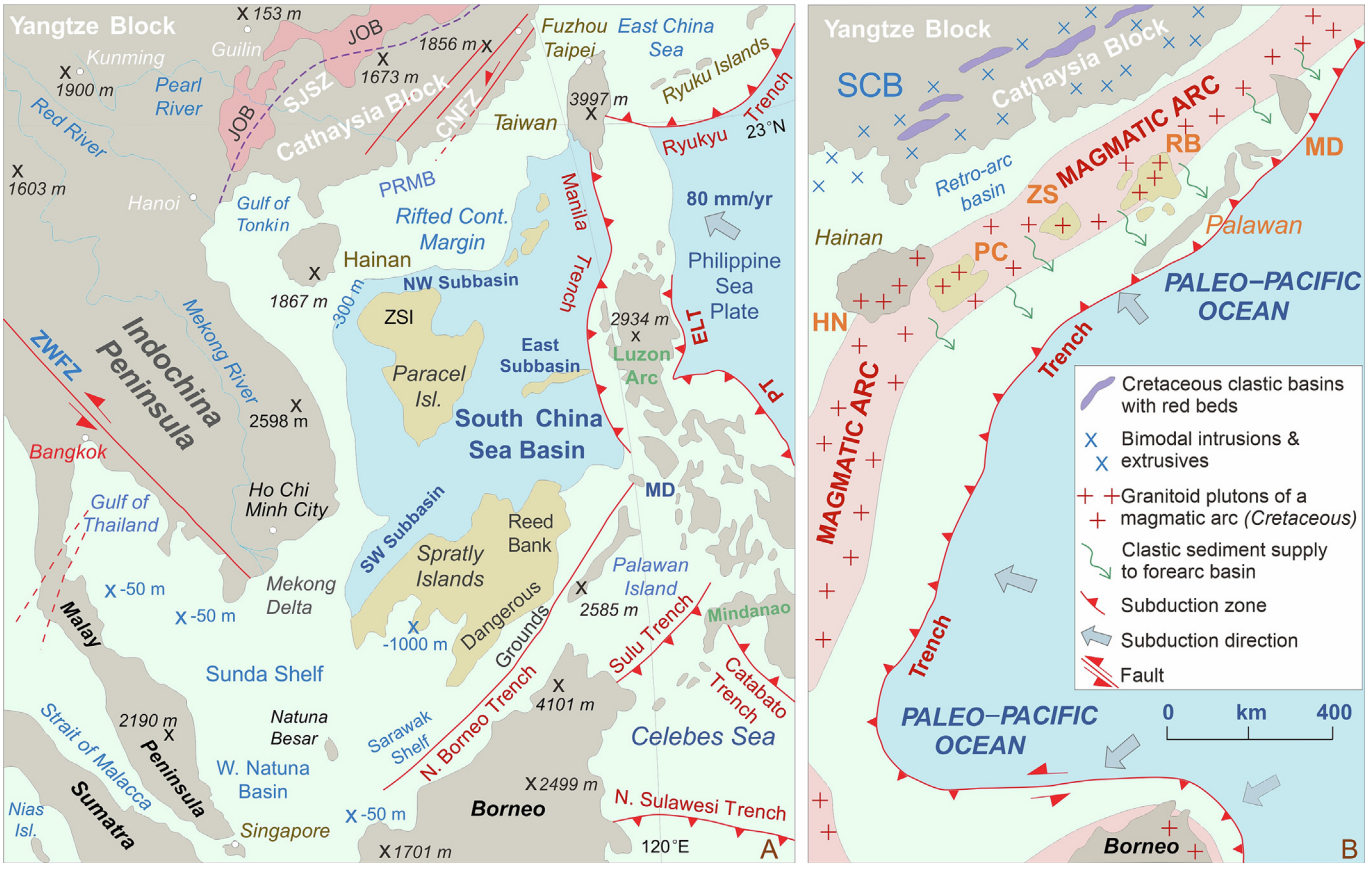

Fig. 12. (A) Simplified tectonic map of modern SE Asia, South China Sea, and its environs. (B) Reconstructed paleogeography of SE Asia and the Cretaceous (~120 Ma) magmatic arc located outboard of the coastal SE Asia (data from: Li et al., 2014a; Zahirovic et al., 2014; Shao et al., 2015; Jiang et al., 2015).

Beibu Gulf Basins to the east and the west of the Hainan Island, and on Taiwan in the NE end of the South China Sea (Fig. 12A) (Yui et al., 1996; Yan et al., 2014; Hennig et al., 2017; Shao et al., 2017; Shao et al., 2019; Cao et al., 2021; Cui et al., 2021; Jin et al., 2022; Xu et al., 2022; Wang et al., 2023). Metamorphosed plutonic rocks with ages of 130–80 Ma in SW Borneo represent the products of the Paleo-Pacific oceanic plate subduction beneath the Indochina–East Malaysia Block during the Cretaceous (Hennig et al., 2017; Wang et al., 2023). Nearly 130–110 Ma granites and doleritic dike intrusions have also been reported from microcontinental blocks in the South China Sea (Nanshan and Zhongsha Islands, and Borneo) (Yan et al., 2010, 2014; Cai et al., 2019; Miao et al., 2021) that were probably once part of the South China Block. The $\varepsilon_{Nd}(t)$ and $\varepsilon_{Hf}(t)$ isotopic values, and geochemical characteristics of Jurassic–Cretaceous mafic to felsic, intrusive and extrusive rock associations in Sabah, in western Borneo, SE Vietnam, and Coastal South China Sea display spatial variations (particularly in their $\varepsilon_{Nd}(t)$ and $\varepsilon_{Hf}(t)$ values, coupled with younging age progression from the NW to the SE (Wang et al., 2023). These features are interpreted to indicate the existence of a major active continental margin arc as a result of the westward (landward-dipping) subduction of the Paleo-Pacific slab (Fig. 12B; Breitfeld et al., 2020; Batara and Xu, 2022; Wang et al., 2023; van de Lagemaat et al., 2024). Trench and slab retreat caused the eastward migration of this magmatic arc and created microcontinental blocks that were rifted away from the mainland Asia and drifted southwards with the opening and spreading of the South China Sea (Suggate et al., 2014; Cui et al., 2021). Detrital fingerprints (including geochemistry, heavy mineral, and zircon U-Pb geochronology) of Mesozoic to Cenozoic strata from Hainan and Palawan Islands, the Pearl River Mouth Basin, and the South China Sea Basin all reveal similar provenance signatures (with age peaks at ca. 120 Ma and ca. 115 Ma), suggesting that there is a geological record of arc magmatism in the region around 120 Ma (Knittel, 2010; Yokoyama et al., 2012; Suggate et al., 2014; Jiang et al., 2015; Padrones et al., 2017; Shao et al., 2017; Yan et al., 2018; Cao et al., 2021; Cui et al., 2021).

Previous studies have proposed that a ca. 120 Ma magmatic arc existed on the margin of the South China Block and possibly outboard (Jiang et al., 2015). The late Mesozoic igneous rocks found along the South China Sea margins can be geochemically and geochronologically correlated with those widely distributed in the surrounding landmasses, representing a possible continuous continental arc system outboard of Southeast Asia (Fig. 12B and **Supplementary Data Fig. S1**; Yan et al., 2014; Hennig et al., 2017; Shao et al., 2017; Xu et al., 2017; Cui et al., 2021). Combined with the extant geochronological and geochemical data from Cretaceous magmatic rocks on Hainan and SE China, our new results support the occurrence of an Andean-type magmatic arc along and offshore of SE China throughout the late Cretaceous (Fig. 12B). Lithological assemblages, sedimentary structures, provenance signatures, and the geochronology of detrital minerals indicate, for example, that the West Philippines microcontinent was attached to and was contiguous with mainland China until the Oligocene, when the opening of the South China Sea began (Fig. 12B; Shao et al., 2017; Chen et al., 2019; Cao et al., 2021;

Wei et al., 2023). Thus, the geological evidence from the mainland South China and other continental fragments within the South China Sea points to continued subduction–related magmatism in this region, including Hainan and other microcontinental blocks in the South China Sea.

6.5. Was there a magmatic quiescence stage in SE China and Hainan during the Aptian (125–115 Ma)?

Based on the available magmatic zircon U-Pb ages from the continental SE China (Fig. 10A) some geologists have proposed a nearly 10-million year–long magmatic quiescence period (or magmatic lull) between 125 Ma and 115 Ma in the Early Cretaceous. The timing of this inferred magmatic quiescence seems to be consistent with the absence of ~ 120 Ma detrital zircons in all major river systems in South China (Jiang et al., 2015). Some of the current interpretations for the lack of magmatism during this time include: slab window opening due to the break-off of the subducting slab (Li et al., 2014a, 2020) and the collision between a hypothetical micro-continent (e.g., the West Philippine microcontinent) and the SE China continental margin (Faure et al., 1989; Chu et al., 2020; Wei et al., 2023). Considering the deformation and metamorphism that occurred in the Changle-Nan'ao Metamorphic Belt (CNMB) as documented by macroscopic and microscopic structures (Wei et al., 2015, 2023), the emplacement of *syn*-tectonic plutons (with oriented minerals) during 130–105 Ma (Li et al., 2015; Wei et al., 2023; Zhou et al., 2023), the angular unconformity between ca. 140–130 Ma and ca. 110–90 Ma volcanic rocks in southeast China (Guo et al., 2012b; Li et al., 2018), and the Early Cretaceous ophiolites exposed in the Mindoro Island (Yumul, 2007) and involved in S-directed thrusting, it seems likely that the collision between the South China block and the West Philippines microcontinent caused the NW–SE shortening regime around CNMB and halted magmatism temporarily and creating a pause in magmatic output (Faure et al., 1989; Wei et al., 2015, 2023). More field-based, regional geological, geochronological, isotopic, and geophysical studies have to be conducted to test these two hypotheses. The question of the real cause of the apparent Aptian gap in magmatism in the region is beyond the scope of our current study.

However, it is important to point out that the 120 Ma granites and detrital zircons on Hainan appear to overlap in time with the inferred ~ 125 Ma to 115 Ma "magmatic quiescence" period in mainland southern China. Furthermore, our discovery of a ~ 117 Ma high-K, calc-alkaline I-type granite on Hainan suggests that there was some magmatic activity in the region during this time. Thus, our data from Hainan does not support the possible existence of a magmatic quiescence period in SE China during the Aptian. It is possible that the apparent lack of Aptian magmatic rocks in parts of SE China may also be either due to their local absence or poor documentation in the geological record. Alternatively, this 10 m.y. period of magmatic lull was a result of accelerated, trench–normal slab velocity of the Paleo–Pacific Plate, causing flattening of the subduction angle that, in turn, might have inhibited hydrous melting and associated magmatism in the upper plate (Dilek and Tang, 2021), or the collision between the South China Block and the West Philippines microcontinent (Wei et al., 2023). Hainan Island and the micro-continental blocks in the *peri*-South China Sea are outside the range of the flattening subduction angle or crustal shortening regime due to the arrival of a microcontinent carried by the subduction slab, the continuing subduction of the Paleo-Pacific plate leading to the continuous magmatic activity. Further field–based structural mapping and precise geochronological studies of Cretaceous magmatic rocks in SE China and on the islands in the South China Sea are needed to test all currently available hypotheses.

7. Conclusions

We draw the following conclusions based on the results of our integrated in-situ zircon U-Pb and Hf-O isotope analyses, and whole-rock major, trace element, and Sr-Nd isotope analyses of Cretaceous granites on Hainan Island, and on our synthesis of the compilation of the extant geological, geochemical, and geochronological data from SE China and from the continental fragments in the South China Sea.

(i) Cretaceous granitic magmatism on the island of Hainan developed during three discrete pulses at 135 Ma, 120–90 Ma, and around 70 Ma. The Hainan granitoids are all high-K, calc-alkaline granites with an I-type geochemical affinity, typical of magmatic arc granites. Their $\varepsilon_{Hf}(t)$ values show increasing trends with younging in crystallization ages, indicating more contribution of juvenile components into their melt regime through time. These geochemical signatures and the correlation between the $\varepsilon_{Hf}(t)$ and $\delta^{18}O$ values point to the effects of crustal reworking in the late Mesozoic magmatism in SE China.

(ii) The occurrence of Early to Late Cretaceous granitoid rocks in mainland SE China, on the Hainan, Taiwan, and Palawan Islands, and in continental fragments near the northern margin of the South China Sea points to the development of a magmatic arc above the Paleo-Pacific oceanic slab, which was dipping northward beneath the Asian continent during the Cretaceous. Much of the geological record of this arc was fragmented and obliterated as a result of tectonic processes associated with the opening of the South China Sea during the Cenozoic.

(iii) The identification of ca. 117 Ma granodiorite pluton on Hainan Island and other magmatic rocks and nearly coeval detrital zircon ages from the West Philippines microcontinent, Taiwan, and other continental blocks in the northern part of the South China Sea (i.e., Zhongsha and Nansha Blocks) indicate that subduction zone magmatism was ongoing in SE Asia during the Aptian (~125 Ma to 115 Ma), a time period that has been widely considered as magmatically null (so-called "magmatic quiescence"). In light of our new findings and a regional correlation of magmatic events presented in this study, we deduce that the subduction of the Paleo-Pacific oceanic plate beneath SE Asia and the spatially associated flux-melting magmatism must have continued well into the Late Cretaceous. Further precise geochronological studies of Cretaceous plutonic and volcanic rocks in the continental SE China and in the microcontinents within the periphery of the South China Sea are needed to rule out the purported, Aptian "magmatic quiescence" event.

CRediT authorship contribution statement

Xiao-Yan Jiang: Formal analysis, Funding acquisition, Investigation, Methodology, Software, Visualization, Writing – original draft, Conceptualization, Project administration. **Yildirim Dilek:** Data curation, Visualization, Writing – review & editing, Funding acquisition. **Xian-Hua Li:** Funding acquisition, Resources, Supervision, Writing – review & editing, Conceptualization.

Declaration of Competing Interest

The authors declare that they have no known competing financial interests or personal relationships that could have appeared to influence the work reported in this paper.

Acknowledgements

We thank Mulong Chen, Jianbo Zhou, Zechao Chen, Yu Liu, Guoqiang Tang, and Yueheng Yang, for their assistance in our fieldwork, zircon U-Pb age, and Hf-O isotope isotope analyses. Y Dilek's fieldwork on the Hainan Island was supported by funds from the Second Institute of Oceanography and Zhejiang University in Hangzhou that are gratefully acknowledged. This work was supported by the Chinese National Natural Science Foundation (Grant No. 41703010). We acknowledge constructive and insightful reviews by Gaoxue Yang and an anonymous referee that helped us improve the data presentation and interpretations in the paper. We are grateful to Editorial Advisor Prof. M. Santosh for his editorial handling.

Appendix A. Supplementary data

Supplementary data to this article can be found online at https://doi.org/10.1016/j.gsf.2024.101866.

References

Altherr, R., Henjes-Kunst, F., Langer, C., Otto, J., 1999. Interaction between crustal-derived felsic and mantle-derived mafic magmas in the Oberkirch Pluton (European Variscides, Schwarzwald, Germany). Contrib. Mineral. Petrol. 137, 304–322.

Barbarin, B., 1999. A review of the relationships between granitoid types, their origins and their geodynamic environments. Lithos 46 (3), 605–626.

Batara, B., Xu, C., 2022. Evolved magmatic arcs of South Borneo: Insights into Cretaceous slab subduction. Gondwana Res. 111, 142–164.

Breitfeld, H.T., Davies, L., Hall, R., Armstrong, R., Forster, M., Lister, G., Thirlwall, M., Grassineau, N., Hennig-Breigeld, J., van Hattum, M.W., 2020. Mesozoic Paleo-Pacific subduction beneath SW Borneo: U-Pb geochronology of the Schwaner granitoids and the Pinoh metamorphic group. Front. Earth Sci. 8, 568715.

Cai, G.Q., Wan, Z.F., Yao, Y.J., Zhong, L.F., Zheng, H., Kapsiotis, A., Zhang, C., 2019. Mesozoic Northward Subduction Along the SE Asian Continental Margin Inferred from Magmatic Records in the South China Sea. Minerals 9, 598.

Cao, L.C., Shao, L., Qiao, P.J., Cui, Y.C., Zhang, G.C., Zhang, X.T., 2021. Formation and paleogeographic evolution of the Palawan continental terrane along the Southeast Asian margin revealed by detrital fingerprints. GSA Bulletin 133 (5–6), 1167–1193.

Cao, X.Z., Zahirovic, S., Li, S.Z., Suo, Y.H., Wang, P.C., Liu, J.P., Müller, R.D., 2022. A deforming plate tectonic model of the South China Block since the Jurassic. Gondwana Res. 102, 3–16.

Chappell, B.W., White, A.J.R., 1974. Two contrasting granite types. Pacific Geology 8, 173–174.

Chappell, B.W., White, A.J.R., 1992. I-and S-type granites in the Lachlan Fold Belt. Earth Environ Sci Trans R Soc Edinb 83 (1–2), 1–26.

Chappell, B.W., White, A.J.R., Williams, I.S., Wyborn, D., Wyborn, L.A.I., 2000. Lachlan Fold Belt granites revisited: high-and low-temperature granites and their implications. Aust. J. Earth Sci 47 (1), 123–138.

Chappell, B.W., White, A.J., 2001. Two contrasting granite types: 25 years later. Aust. J. Earth Sci 48 (4), 489–499.

Chappell, B.W., Bryant, C.J., Wyborn, D., White, A.J.R., Williams, I.S., 1998. High- and low- temperature I-type granites. Resour. Geol 48 (4), 225–235.

Chappell, B.W., White, A.J.R., Williams, I.S., Wyborn, D., 2004. Low-and high-temperature granites. Earth Environ. Sci. Trans. R Soc. Edinb. 95 (1–2), 125–140.

Charvet, J., Lapierre, H., Yu, Y., 1994. Geodynamic significance of the Mesozoic volcanism of southeastern China. J Asian Earth Sci 9, 387–396.

Charvet, J., Shu, L., Shi, Y., Guo, L., Faure, M., 1996. The building of south China: collision of Yangzi and Cathaysia blocks, problems and tentative answers.J. Southeast Asian. Earth Sci 13 (3–5), 223–235.

Chen, C.H., Lin, W., Lan, C.Y., Lee, C.Y., 2004. Geochemical, Sr and Nd isotopic characteristics and tectonic implications for three stages of igneous rock in the Late Yanshanian (Cretaceous) orogeny, SE China. Earth Environ Sci Trans R Soc Edinb 95 (1–2), 237–248.

Chen, C.H., Lee, C.Y., Lin, J.W., Chu, M.F., 2019. Provenance of sediments in western Foothills and Hsuehshan Range (Taiwan): A new view based on the EMP monazite versus LA-ICPMS zircon geochronology of detrital grains. Earth Sci Rev 190, 224–246.

Chen, M.L., Li, S.X., Zeng, Y.L., Zhou, J.B., 2008. Petrochemical characteristics and metallogenic analysis of the Cretaceous Qianjia rock bodies in Hainan Island. Mineral Resour. Geol. 22, 36–42. in Chinese with English Abstract.

Chen, M.L., Ma, C.Q., Lv, Z.Y., Yun, P., Liu, Y.Y., 2014b. Zircon U-Pb chronology and geological significance of Qianjia Complex pluton, Hainan Island. Geological Science and Technology Information 33, 1–10. in Chinese with English Abstract.

Chen, J.Y., Yang, J.H., Zhang, J.H., Sun, J.F., Wilde, S.A., 2013. Petrogenesis of the Cretaceous Zhangzhou batholith in southeastern China: Zircon U-Pb age and Sr–Nd–Hf–O isotopic evidence. Lithos 162, 140–156.

Chen, J.Y., Yang, J.H., Zhang, J.H., Sun, J.F., 2014a. Geochemical transition shown by Cretaceous granitoids in southeastern China: Implications for continental crustal reworking and growth. Lithos 196, 115–130.

Chen, J.Y., Yang, J.H., Zhang, J.H., Sun, J.F., Zhu, Y.S., Hartung, E., 2022. Generation of Cretaceous high-silica granite by complementary crystal accumulation and silicic melt extraction in the coastal region of southeastern China. GSA Bulletin 134 (1–2), 201–222.

Chu, Y., Lin, W., Faure, M., Xue, Z., Ji, W., Feng, Z., 2019. Cretaceous episodic extension in the south China block, east Asia: Evidence from the Yuechengling massif of central south China. Tectonics 38 (10), 3675–3702.

Chu, Y., Lin, W., Faure, M., Allen, M.B., Feng, Z., 2020. Cretaceous exhumation of the Triassic intracontinental Xuefengshan Belt: Delayed unroofing of an orogenic plateau across the South China Block? Tectonophysics 793, 228592.

Chung, S.L., Sun, S.S., Tu, K., Chen, C.H., Lee, C.Y., 1994. Late Cenozoic basaltic volcanism around the Taiwan Strait, SE China: Product of lithosphere-asthenosphere interaction during continental extension. Chem. Geol. 112 (1–2), 1–20.

Chung, S.L., Jahn, B.M., Chen, S.J., Lee, T., Chen, C.H., 1995. Miocene basalts in northwestern Taiwan: Evidence for EM-type mantle sources in the continental lithosphere. Geochim. Cosmochim. Acta 59 (3), 549–555.

Chung, S.L., Cheng, H., Jahn, B.M., O'Reilly, S.Y., Zhu, B., 1997. Major and trace element, and Sr-Nd isotope constraints on the origin of Paleogene volcanism in South China prior to the South China Sea opening. Lithos 40 (2–4), 203–220.

Collins, W.J., Belousova, E.A., Kemp, A.I., Murphy, J.B., 2011. Two contrasting Phanerozoic orogenic systems revealed by hafnium isotope data. Nat. Geosci. 4 (5), 333–337.

Collins, W.J., Huang, H.Q., Jiang, X.Y., 2016. Water-fluxed crustal melting produces Cordilleran batholiths. Geology 44, 143–146.

Cui, Y., Shao, L., Li, Z.X., Zhu, W., Qiao, P., Zhang, X., 2021. A Mesozoic Andean-type active continental margin along coastal South China: New geological records from the basement of the northern South China Sea. Gondwana Res. 99, 36–52.

Dall'Agnol, R., Teixeira, N.P., Rämö, O.T., Moura, C.A.V., Macambira, M.J.B., Oliveira, D.C., 2005. Petrogenesis of the Paleoproterozoic, rapakivi, A-type granites of the Archean Carajás Metallogenic Province, Brazil. Lithos 80, 101–129.

Deng, Z.B., Liu, S.W., Zhang, L.F., Wang, Z.Q., Wang, W., Yang, P.T., Luo, P., Guo, B.R., 2014. Geochemistry, zircon U-Pb and Lu–Hf isotopes of an Early Cretaceous intrusive suite in northeastern Jiangxi Province, South China Block: Implications for petrogenesis, crust/mantle interactions and geodynamic processes. Lithos 200, 334–354.

DePaolo, D.J., 1981. Trace element and isotopic effects of combined wallrock assimilation and fractional crystallization. Earth Planet. Sci. Lett. 53 (2), 189–202.

Dhuime, B., Hawkesworth, C., Cawood, P., 2011. When continents formed. Science 331 (6014), 154–155.

Dilek, Y., Tang, L., 2021. Magmatic record of the Mesozoic geology of Hainan Island and its implications for the Mesozoic tectonomagmatic evolution of SE China: effects of slab geometry and dynamics in continental tectonics. Geol. Mag. 158, 118–142.

Dong, C.W., Zhou, X.M., Li, H.M., Ren, S.L., Zhou, X.H., 1997. Late Mesozoic crust-mantle interaction in southeastern Fujian: isotopic evidence from the Pingtan igneous complex. Chin. Sci. Bullet. 42, 495–498. in Chinese with English Abstract.

Faure, M., Marchadier, Y., Rangin, C., 1989. Pre-Eocene synmetamorphic structure in the Mindoro-Romblon-Palawan area, west Philippines, and implications for the history of southeast Asia. Tectonics 8, 963–979.

Frost, B.R., Arculus, R.J., Barnes, C.G., Collins, W.J., Ellis, D.J., Frost, C.D., 2001. A geochemical classification of granitic rocks. J. Petrol. 42, 2033–2048.

Ge, X.Y., Li, X.H., Zhou, H.W., 2003. Geochronologic, geochemistry and Sr–Nd isotopes of the Late Cretaceous mafic dike swarms in southern Hainan Island. Geochimica 32 (1), 11–20.

Ge, X.Y., 2003. Mesozoic Magmatism in Hainan Island (SE China) and Its Tectonic Significance: Geochronology, Geochemistry and Sr-Nd Isotope Evidence. Ph.D. Thesis, Chinese Academy of Sciences, Beijing, China, pp. 1–87 (in Chinese with English abstract).

Gilder, S.A., Keller, G.R., Luo, M., Goodell, P.C., 1991. Eastern Asia and the western Pacific timing and spatial distribution of rifting in China. Tectonophysics 197 (2–4), 225–243.

Griffin, W.L., Pearson, N.J., Belousova, E., Jackson, S.E., van Achterbergh, E., O'Reilly, S.Y., Shee, S.R., 2000. The Hf isotope composition of cratonic mantle: LAM-MCICPMS analysis of zircon megacrysts in kimberlites. Geochim. Cosmochim. Acta 64, 133–147.

Guo, C.L., Chen, Y.C., Zeng, Z.L., Lou, F.S., 2012a. Petrogenesis of the Xihuashan granites in southeastern China: Constraints from geochemistry and in-situ analyses of zircon U-Pb-Hf-O isotopes. Lithos 148, 209–227.

Guo, F., Fan, W.M., Li, C.W., Zhao, L., Li, H.X., Yang, J.H., 2012b. Multi-stage crust–mantle interaction in SE China: temporal, thermal and compositional constraints from the Mesozoic felsic volcanic rocks in eastern Guangdong-Fujian provinces. Lithos 150, 62–84.

He, H.Y., Wang, Y.J., Cawood, P.A., Qian, X., Zhang, Y.Z., Zhao, G.F., 2020. Permo–Triassic granitoids, Hainan Island, link to Paleotethyan not Paleopacific tectonics. Bulletin 132(9-10), 2067-2083.

He, Z.Y., Xu, X.S., Yu, Y., Zou, H.B., 2009. Origin of the Late Cretaceous syenite from Yandangshan, SE China, constrained by zircon U-Pb and Hf isotopes and geochemical data. Int. Geol. Rev. 51 (6), 556–582.
He, Z.Y., Xu, X.S., Niu, Y.L., 2010. Petrogenesis and tectonic significance of a Mesozoic granite–syenite–gabbro association from inland South China. Lithos 119, 621–641.
He, Z.Y., Xu, X.S., 2012. Petrogenesis of the Late Yanshanian mantle-derived intrusions in southeastern China: response to the geodynamics of paleo-Pacific plate subduction. Chem. Geol. 328, 208–221.
Hennig, J., Breitfeld, H.T., Hall, R., Nugraha, A.S., 2017. The Mesozoic tectono-magmatic evolution at the Paleo-Pacific subduction zone in West Borneo. Gondwana Res. 48, 292–310.
Ho, K.S., Chen, J.C., Lo, C.H., Zhao, H.L., 2003. ^{40}Ar-^{39}Ar Dating and Geochemical Characteristics of Late Cenozoic Basaltic Rocks from the Zhejiang-Fujian Region, SE China: Eruption Ages, Magma Evolution and Petrogenesis. Chem. Geol. 197 (1–4), 287–318.
Huang, H.Q., Li, X.H., Li, Z.X., Li, W.X., 2015. Formation of the Jurassic South China Large Granitic Province: insights from the genesis of the Jiufeng pluton. Chem. Geol. 401, 43–58.
Huang, C.Y., Yen, Y., Zhao, Q., Lin, C.T., 2012. Cenozoic stratigraphy of Taiwan: Window into rifting, stratigraphy and paleoceanography of South China Sea. Chin. Sci. Bull 57, 3130–3149.
Jahn, B.M., Zhou, X.H., Li, J.L., 1990. Formation and tectonic evolution of Southeastern China and Taiwan: isotopic and geochemical constraints. Tectonophysics 183, 145–160.
Jiang, X.Y., Li, X.H., 2014. In situ zircon U-Pb and Hf–O isotopic results for ca. 73 Ma granite in Hainan Island: Implications for the termination of an Andean-type active continental margin in southeast China. J Asian Earth Sci 82, 32–46.
Jiang, X.Y., Li, X.H., Collins, W.J., Huang, H.Q., 2015. U-Pb age and Hf-O isotopes of detrital zircons from Hainan Island: Implications for Mesozoic subduction models. Lithos 239, 60–70.
Jiang, X.Y., Ling, M.X., Wu, K., Zhang, Z.K., Sun, W.D., Sui, Q.L., Xia, X.P., 2018a. Insights into the origin of coexisting A_1-and A_2-type granites: Implications from zircon Hf-O isotopes of the Huayuangong intrusion in the Lower Yangtze River Belt, eastern China. Lithos 318, 230–243.
Jiang, X.Y., Luo, J.C., Guo, J., Wu, K., Zhang, Z.K., Sun, W.D., Xia, X.P., 2018b. Geochemistry of I-and A-type granites of the Qingyang-Jiuhuashan complex, eastern China: Insights into early Cretaceous multistage magmatism. Lithos 316, 278–294.
Jiang, D.S., Xu, X.S., Wang, X.J., Zeng, G., Chen, A.X., Huang, B., Huang, F., 2021. Geochemical evidence for the Paleo-Pacific plate subduction at ~125 Ma in Eastern China. Lithos 398, 106259.
Jiang, Y.H., Zhao, P., Zhou, Q., Liao, S.Y., Jin, G.D., 2011. Petrogenesis and tectonic implications of Early Cretaceous S- and A-type granites in the northwest of the Gan-Hang rift. SE China. Lithos 121 (1–4), 55–73.
Jin, H.L., Wan, S.M., Clift, P.D., Liu, C., Huang, J., Jiang, S.J., Li, M.J., Qin, L., Shi, X.F., Li, A.C., 2022. Birth of the Pearl River at 30 Ma: Evidence from sedimentary records in the northern South China Sea. Earth Planet. Sci. Lett. 600, 117872.
Kemp, A.I.S., Hawkesworth, C.J., Paterson, B.A., Kinny, P.D., 2006. Episodic growth of the Gondwana supercontinent from hafnium and oxygen isotopes in zircon. Nature 439 (7076), 580–583.
Kemp, A.I.S., Hawkesworth, C.J., Collins, W.J., Gray, C.M., Blevin, P.L., 2009. Isotopic evidence for rapid continental growth in an extensional accretionary orogen: The Tasmanides, eastern Australia. Earth Planet. Sci. Lett. 284 (3–4), 455–466.
King, P.L., Chappell, B.W., Allen, C.M., White, A.J.R., 2001. Are A-type granites the high-temperature felsic granites? Evidence from fractionated granites of the Wangrah Suite. Aust. J. Earth Sci 48 (4), 501–514.
Knittel, U., 2010. 83 Ma rhyolite from Mindoro-evidence for Late Yanshanian magmatism in the Palawan Continental Terrane (Philippines). Isl Arc 20, 138–146.
Lan, C.Y., Lee, T., Jahn, B.M., Yui, T.F., 1995. Taiwan as a witness of repeated mantle inputs – Sr-Nd-O isotopic geochemistry of Taiwan granitoids and metapelites. Chem. Geol. 124, 287–303.
Lapierre, H., Jahn, B.M., Charvet, J., Yu, Y.W., 1997. Mesozoic felsic arc magmatism and continental olivine tholeiites in Zhejiang Province and their relationship with the tectonic activity in southeastern China. Tectonophysics 274, 321–338.
Li, X.H., 2000. Cretaceous magmatism and lithospheric extension in Southeast China. J. Asian Earth Sci. 18, 293–305.
Li, X.H., 2002. Geochemical and Sm-Nd isotopic characteristics of metabasites from central Hainan Island, South China and their tectonic significance. Isl Arc 11, 193–205.
Li, J.H., Cawood, P.A., Ratschbacher, L., Zhang, Y.Q., Dong, S.W., Xin, Y.J., Yang, H., Zhang, P.X., 2020. Building Southeast China in the late Mesozoic: Insights from alternating episodes of shortening and extension along the Lianhuashan fault zone. Earth Sci. Rev. 201, 103056.
Li, B., Jiang, S.Y., Zhang, Q., Zhao, H.X., Zhao, K.D., 2015a. Cretaceous crust–mantle interaction and tectonic evolution of Cathaysia Block in South China: Evidence from pulsed mafic rocks and related magmatism. Tectonophysics 661, 136–155.
Li, W.X., Li, X.H., Li, Z.X., 2005. Neoproterozoic bimodal magmatism in the Cathaysia Block of South China and its tectonic significance. Precambrian Res. 136, 51–66.
Li, Z.X., Li, X.H., 2007. Formation of the 1300-km-wide intracontinental orogen and postorogenic magmatic province in Mesozoic South China: A flat-slab subduction model. Geology 35, 179–182.
Li, Z.X., Li, X.H., Zhou, H., Kinny, P.D., 2002. Grenvillian continental collision in south China: new SHRIMP U-Pb zircon results and implications for the configuration of Rodinia. Geology 30, 163–166.
Li, X.H., Li, Z.X., Li, W.X., Wang, Y., 2006. Initiation of the Indosinian Orogeny in South China: evidence for a Permian Magmatic Arc on Hainan Island. J. Geol 114, 341–353.
Li, X.H., Li, Z.X., Li, W.X., Liu, Y., Yuan, C., Wei, G.J., Qi, C.S., 2007. U-Pb zircon, geochemical and Sr–Nd–Hf isotopic constraints on age and origin of Jurassic I- and A-type granites from central Guangdong, SE China: a major igneous event in response to foundering of a subducted flat-slab? Lithos 96 (1–2), 186–204.
Li, Z.X., Li, X.H., Li, W.X., Ding, S., 2008. Was Cathaysia part of Proterozoic Laurentia?—New data from Hainan Island, South China. Terra Nova 20, 154–164.
Li, Q.L., Li, X.H., Liu, Y., Tang, G.Q., Yang, J.H., Zhu, W.G., 2010b. Precise U-Pb and Pb-Pb dating of Phanerozoic baddeleyite by SIMS with oxygen flooding technique. J. Anal. Spectrom. 25, 1107–1113.
Li, X.H., Li, W.X., Wang, X.C., Li, Q.L., Liu, Y., Tang, G.Q., Gao, Y.Y., Wu, F.Y., 2010a. SIMS U–Pb zircon geochronology of porphyry Cu–Au–(Mo) deposits in the Yangtze River Metallogenic Belt, eastern China: magmatic response to early Cretaceous lithospheric extension. Lithos 119, 427–438.
Li, X.H., Li, W.X., Li, Q.L., Wang, X.C., Liu, Y., Yang, Y.H., 2010c. Petrogenesis and tectonic significance of the ca.850 Ma Gangbian alkaline complex in South China: evidence from in situ zircon U-Pb dating, Hf-O Isotopes and Whole-Rock Geochemistry. Lithos 114, 1–15.
Li, X.H., Li, Z.X., He, B., Li, W.X., Li, Q.L., Gao, Y., Wang, X.C., 2012. The Early Permian active continental margin and crustal growth of the Cathaysia Block: in situ U-Pb, Lu-Hf and O isotope analyses of detrital zircons. Chem. Geol. 328, 195–207.
Li, X.Y., Li, S.Z., Suo, Y.H., Dai, L.M., Guo, L.L., Ge, F.J., Lin, P.J., 2018. Late Cretaceous basalts and rhyolites from Shimaoshan group in eastern Fujian Province, SE China: Age, petrogenesis, and tectonic implications. Int. Geol. Rev. 60 (11–14), 1721–1743.
Li, X.H., Liu, Y., Li, Q.L., Guo, C.H., Chamberlain, K.R., 2009. Precise determination of Phanerozoic zircon Pb/Pb age by multicollector SIMS without external standardization. Geochemistry, Geophy. Geosystems 10, Q04010.
Li, X.H., Long, W.G., Li, Q.L., 2010d. Penglai zircon megacrysts: a potential new working reference material for microbeam determination of Hf–O isotopes and U–Pb Age. Geostand. Geoanal. Res. 34, 117–134.
Li, Y., Ma, C.Q., Xing, G.F., Zhou, H.W., 2015. The Early Cretaceous evolution of SE China: Insights from the Changle–Nan'ao Metamorphic Belt. Lithos 230, 94–104.
Li, Z., Qiu, J.S., Yang, X.M., 2014b. A review of the geochronology and geochemistry of Late Yanshanian (Cretaceous) plutons along the Fujian coastal area of southeastern China: Implications for magma evolution related to slab break-off and rollback in the Cretaceous. Earth Sci Rev 128, 232–248.
Li, X.H., Tang, G.Q., Gong, B., Yang, Y.H., Hou, K.J., Hu, Z.C., Li, Q.L., Liu, Y., Li, W.X., 2013. Qinghu zircon: a working reference for microbeam analysis of U-Pb age and Hf and O isotopes. Chin. Sci. Bull 58, 4647–4654.
Li, X., Wei, J.H., Li, Y.J., Zhai, Y.L., 2016. Zircon U-Pb Age and Geochemical and Nd-Hf Isotopic Constraints on the Origin of the Early Cretaceous Shilu A-type Granite in Hainan Island, South China. Geotecton. Metallogen. 3, 587–602. in Chinese with English Abstract.
Li, J.H., Zhang, Y.Q., Dong, S.W., Johnston, S.T., 2014a. Cretaceous tectonic evolution of South China: A preliminary synthesis. Earth Sci. Rev. 134, 98–136.
Liu, J.L., Ni, J.L., Chen, X.Y., Craddock, J.P., Zheng, Y.Y., Ji, L., Hou, C.R., 2021. Early Cretaceous tectonics across the North Pacific: New insights from multiphase tectonic extension in Eastern Eurasia. Earth Sci. Rev. 217, 103552.
Liu, J.Q., Ren, Z.Y., Nichols, A.R.L., Song, M.S., Qian, S.P., Zhang, Y., Zhao, P.P., 2015. Petrogenesis of Late Cenozoic basalts from North Hainan Island: Constraints from melt inclusions and their host olivines. Geochim. Cosmochim. Acta 152, 89–121.
Liu, L., Xu, X.S., Xia, Y., 2014. Cretaceous Pacific plate movement beneath SE China: Evidence from episodic volcanism and related intrusions. Tectonophysics 614, 170–184.
Liu, Q., Yu, J.H., Wang, Q., Su, B., Zhou, M.F., Xu, H., Cui, X., 2012. Ages and geochemistry of granites in the Pingtan-Dongshan Metamorphic Belt, Coastal South China: new constraints on Late Mesozoic magmatic evolution. Lithos 150, 268–286.
Loiselle, M.C., Wones, D.R., 1979. Characteristics and origin of anorogenic granites. Abstract Programs - Geol Soc Am Bull 11, 468.
Ludwig, K.R., 2008. Users' manual for Isoplot 3.70: a geochronological toolkit for Mircrosoft Excel. Berkeley Geochronology Center Special Publication No. 4. Berkeley, California.
Mao, J.R., Chen, R., Li, J.Y., Ye, H.M., Zhao, X.L., 2006. Geochronology and geochemical characteristics of Late Mesozoic granitic rocks from southwestern Fujian and their tectonic evolution. Acta Petrol. Sin. 22 (6), 1723–1734. in Chinese with English abstract.
Mao, J.W., Cheng, Y.B., Chen, M.H., Pirajno, F., 2013. Major types and time-space distribution of Mesozoic ore deposits in South China and their geodynamic settings. Miner. Depos. 48, 267–294.
Meng, L., Li, Z.X., Chen, H., Li, X.H., Wang, X.C., 2012. Geochronological and geochemical results from Mesozoic basalts in southern South China Block support the flat-slab subduction model. Lithos 132, 127–140.
Metcalfe, I., 2009. Late Palaeozoic and Mesozoic tectonic and palaeogeographical evolution of SE Asia. Late Palaeozoic and Mesozoic Ecosystems in SE Asia. Geol. Soc. Lond. Spec. Publ. 315, 7–23.
Miao, X.Q., Huang, X.L., Yan, W., Yang, F., Zhang, W.F., Yu, Y., Cai, Y.X., Zhu, S.Z., 2021. Two episodes of Mesozoic mafic magmatism in the Nansha Block: Tectonic transition from continental arc to back-arc basin. Lithos 404, 106502.

Miller, C.F., McDowell, S.M., Mapes, R.W., 2003. Hot and cold granites? Implications of zircon saturation temperatures and preservation of inheritance. Geology 31 (6), 529–532.
Montel, J.M., Vielzeuf, D., 1997. Partial melting of metagreywackes, part II. Compositions of minerals and melts. Contrib. Miner. Petrol. 128, 176–196.
Nasdala, L., Hofmeister, W., Norberg, N., Mattinson, J.M., Corfu, F., Dörr, W., Kamo, S. L., Kennedy, A.K., Kronz, A., Reiners, P.W., Frei, D., Kosler, J., Wan, Y., Götze, J., Häger, T., Kröner, A., Valley, J.W., 2008. Zircon M257—a homogeneous natural reference material for the ion microprobe U-Pb analysis of zircon. Geostand. Geoanal. Res. 32, 47–265.
Padrones, J.T., Tani, K., Tsutsumi, Y., Imai, A., 2017. Imprints of late Mesozoic tectono-magmatic events on Palawan continental block in northern Palawan, Philippines. J. Asian Earth Sci. 142, 56–76.
Page, F.Z., Fu, B., Kita, N.T., Fournelle, J., Spicuzza, M.J., Schulze, D.J., Viljoen, F., Basei, M.A.S., Valley, J.W., 2007. Zircons from kimberlite: new insights from oxygen isotopes, trace elements, and Ti in zircon thermometry. Geochim. Cosmochim. Acta 71 (15), 3887–3903.
Patiño Douce, A.E., 1999. What do experiments tell us about the relative contributions of crust and mantle to the origin of granitic magmas? Geol. Soc., Lond Spec. Publ. 168, 55–75.
Patiño Douce, A.E., McCarthy, T.C., 1998. Melting of crustal rocks during continental collision and subduction. In: Hacker, B.R., Liou, J.G. (Eds.), When Continents Collide: Geodynamics and Geochemistry of Ultrahigh-Pressure Rocks. Springer, Dordrecht, pp. 27–55.
Pearce, J.A., Harris, N.B., Tindle, A.G., 1984. Trace element discrimination diagrams for the tectonic interpretation of granitic rocks. J. Petrol 25 (4), 956–983.
Peng, H.W., Fan, H.R., Jiang, P., Hu, H.L., Lan, T.G., 2021. Two-stage rollbacks of the paleo-Pacific plate beneath the Cathaysia block during Cretaceous: Insights from A-type granites and volcanic rocks. Gondwana Res. 97, 158–175.
Qi, Y.Q., Hu, R.Z., Liu, S., Coulson, I.M., Qi, H.W., Tian, J.J., Feng, C.X., Wang, T., 2012. Geochemical and Sr–Nd–Pb isotopic compositions of Mesozoic mafic dikes from the Gan-Hang tectonic belt, South China: petrogenesis and geodynamic significance. Int. Geol. Rev. 54, 920–939.
Qiu, J.S., Xiao, E., Jian, H., Xu, X.S., Jiang, S.Y., Li, Z., 2008. Petrogenesis of highly fractionated I-type granites in the coastal area of northeastern Fujian Province: Constraints from zircon U-Pb geochronology, geochemistry and Nd-Hf isotopes. Acta Petrol. Sin. 24 (11), 2468–2484. in Chinese with English abstract.
Rapp, R.P., Watson, E.B., 1995. Dehydration melting of metabasalt at 8–32 kbar: implications for continental growth and crust-mantle recycling. J. Petrol. 36 (4), 891–931.
Rapp, R.P., Watson, E.B., Miller, C.F., 1991. Partial melting of amphibolite/eclogite and the origin of Archean trondhjemites and tonalites. Precambrian Res. 51 (1–4), 1–25.
Roberts, P.M., Clemens, J.D., 1993. Origin of high-potassium, talc-alkaline, I-type granitoids. Geology 21, 825–828.
Shao, L., Cao, L.C., Qiao, P.J., Zhang, X.T., Li, Q.Y., van Hinsbergen, D.J., 2017. Cretaceous-Eocene provenance connections between the Palawan Continental Terrane and the northern South China Sea margin. Earth Planet. Sci. Lett. 477, 97–107.
Shao, W.Y., Chung, S.L., Chen, W.S., Lee, H.Y., Xie, L.W., 2015. Old continental zircons from a young oceanic arc, eastern Taiwan: implications for Luzon subduction initiation and Asian accretionary orogeny. Geology 43, 479–482.
Shao, L., Cui, Y., Stattegger, K., Zhu, W., Qiao, P., Zhao, Z., 2019. Drainage control of Eocene to Miocene sedimentary records in the southeastern margin of Eurasian Plate. GSA Bulletin 131 (3–4), 461–478.
Shu, L.S., Faure, M., Yu, J.H., Jahn, B.M., 2011. Geochronological and geochemical features of the Cathaysia block (South China): New evidence for the Neoproterozoic breakup of Rodinia. Precambrian Res 187, 263–276.
Shu, L.S., Yao, J.L., Wang, B., Faure, M., Charvet, J., Chen, Y., 2021. Neoproterozoic plate tectonic process and Phanerozoic geodynamic evolution of the South China Block. Earth Sci. Rev. 216, 103596.
Singh, J., Johannes, W., 1996. Dehydration melting of tonalites. Part II. Composition of melts and solids. Contrib. Miner. Petrol. 125, 26–44.
Sisson, T.W., Ratajeski, K., Hankins, W.B., Glazner, A.F., 2005. Voluminous granitic magmas from common basaltic sources. Contrib. Mineral. Petrol. 148, 635–661.
Sláma, J., Košler, J., Condon, D.J., Crowley, J.L., Gerdes, A., Hanchar, J.M., Horstwood, M.S.A., Morris, G.A., Nasdala, L., Norberg, N., Schaltegger, U., Schoene, B., Tubrett, M.N., Whitehouse, M.J., 2008. Plešovice zircon—a new natural reference material for U-Pb and Hf isotopic microanalysis. Chem. Geol. 249, 1–35.
Stacey, J.S., Kramers, J.D., 1975. Approximation of terrestrial lead isotope evolution by a two-stage model. Earth Planet. Sci. Lett. 26, 207–221.
Suggate, S.M., Cottam, M.A., Hall, R., Sevastjanova, I., Forster, M.A., White, L.T., Armstrong, R.A., Carter, A., Mojares, E., 2014. South China continental margin signature for sandstones and granites from Palawan, Philippines. Gondwana Res. 26 (2), 699–718.
Sun, S.S., McDonough, W.F., 1989. Chemical and isotopic systematics of oceanic basalts: implications for mantle composition and processes. In: Saunders, A.D., Norry, M.J. (Eds.), Magmatism in the Ocean Basins. Geol Soc Spec Publ 42, pp. 313–345.
Sun, S.J., Zhang, L.P., Zhang, R.Q., Ding, X., Zhu, H.L., Zhang, Z.F., Sun, W.D., 2018. Mid–late Cretaceous igneous activity in South China: the Qianjia example, Hainan Island. Int. Geol. Rev. 60, 1665–1683.
Suo, Y.H., Li, S.Z., Jin, C., Zhang, Y., Zhou, J., Li, X., Wang, P.C., Liu, Z., Wang, X.Y., Somerville, I., 2019. Eastward tectonic migration and transition of the Jurassic-Cretaceous Andean-type continental margin along Southeast China. Earth Sci Rev 196, 102884.
Tanaka, T., Togashi, S., Kamioka, H., Amakawa, H., Kagami, H., Hamamoto, T., Yuhara, M., Orihashi, Y., Yoneda, S., Shimizu, H., Kunimaru, T., Takahashi, K., Yanagi, T., Nakano, T., Fujimaki, H., Shinjo, R., Asahara, Y., Tanimizu, M., Dragusanu, C., 2000. JNdi-1: a neodymium isotopic reference in consistency with LaJolla neodymium. Chem. Geol. 168, 279–281.
Tang, L.M., Chen, H.L., Dong, C.W., Shen, Z.Y., Cheng, X.G., Fu, L.L., 2010. Late Mesozoic tectonic extension in SE China: Evidence from the basic dike swarms in Hainan Island. China. Acta Petrol. Sin. 26, 1204–1216. in Chinese with English abstract.
Tang, L.M., Chen, L., Dong, C.W., Yang, S.F., Shen, Z.Y., Cheng, X.G., Fu, L.L., 2013. Middle Triassic post-orogenic extension on Hainan Island: Chronology and geochemistry constraints of bimodal intrusive rocks. Sci. China Earth Sci 56, 783–793.
Tang, L.M., Chen, H.L., Dong, C.W., 2014. Zircon U-Pb dating and tectonic significance of Late Mesozoic granodiorite and its enclaves from Hainan Island. Chinese Journal of Geology 49, 259–274. in Chinese with English abstract.
Thirlwall, M.F., 1991. Long-term reproducibility of multicollector Sr and Nd isotope ratio analysis. Chemical Geology: Isotope Geoscience Section 94 (2), 85–104.
Tian, Z.X., Yan, Y., Huang, C.Y., Dilek, Y., Yu, M.M., Liu, H.Q., Zhang, X.C., Zhang, Y., 2021. Fingerprinting subducted oceanic crust and Hainan Plume in the melt sources of Cenozoic Basalts from the South China Sea Region. Terra Nova 33 (1), 21–29.
Valley, J.W., 2003. Oxygen isotopes in zircon. Reviews in Mineralogy and Geochemistry 53 (1), 343–385.
Valley, J.W., Kinny, P.D., Schulze, D.J., Spicuzza, M.J., 1998. Zircon megacrysts from kimberlite: oxygen isotope variability among mantle melts. Contrib. to Mineral. Petrol. 133, 1–11.
van de Lagemaat, S.H.A., Cao, L., Asis, J., Advokaat, E.L., Mason, P.R.D., Dekkers, M.J., van Hinsbergen, D.J.J., 2024. Causes of Cretaceous subduction termination below South China and Borneo: Was the Proto-South China Sea underlain by an oceanic plateau? Geoscience Frontiers 15, 101752.
Wang, Q., Li, X.H., Jia, X.H., Wyman, D., Tang, G.J., Li, Z.X., Ma, L., Yang, Y.H., Jiang, Z. Q., Guo, G.N., 2012a. Late Early Cretaceous adakitic granitoids and associated magnesian and potassium-richmafic enclaves and dikes in the Tunchang-Fengmu area, Hainan Province (South China): partial melting of lower crust and mantle, and magma hybridization. Chem. Geol. 328, 222–243.
Wang, X.F., Ma, D.Q., Jiang, D.H., Zhang, R.J., Zhang, Q.F., 1991. Geology of Hainan Island (I): Stratigraphic Palaeontology. Geological Publishing House, Beijing, pp. 281 (in Chinese).
Wang, Y.J., Wu, C.M., Zhang, A.M., Fan, W.M., Zhang, Y.H., Zhang, Y.Z., Zhang, Y.Z., Peng, T.P., Yin, C.Q., 2012b. Kwangsian and Indosinian reworking of the eastern South China Block: constraints on zircon U-Pb geochronology and metamorphism of amphibolites and granulites. Lithos 150, 227–242.
Wang, Y.J., Fan, W.M., Zhang, G.W., Zhang, Y.H., 2013. Phanerozoic tectonics of the South China Block: Key observations and controversies. Gondwana Res. 23 (4), 1273–1305.
Wang, Y.J., Qian, J., Bin Asis, J., Cawood, P.A., Wu, S., Zhang, Y., Feng, Q., Lu, X., 2023. "Where, when and why" for the arc-trench gap from Mesozoic Paleo-Pacific subduction zone: Sabah Triassic Cretaceous igneous records in East Borneo. Gondwana Res. 117, 117–138.
Watson, E.B., Harrison, T.M., 1983. Zircon saturation revisited: temperature and composition effects in a variety of crustal magma types. Earth Planet. Sci. Lett. 64, 295–304.
Wei, W., Faure, M., Chen, Y., Ji, W., Lin, W., Wang, Q.C., Yan, Q.R., Hou, Q.L., 2015. Back-thrusting response of continental collision: Early Cretaceous NW-directed thrusting in the Changle-Nan'ao belt (Southeast China). J. Asian Earth Sci 100, 98–114.
Wei, W., Lin, W., Chen, Y., Faure, M., Ji, W.B., Hou, Q.L., Yan, Q.R., Wang, Q.C., 2023. Tectonic controls on magmatic tempo in an active continental margin: Insights from the Early Cretaceous syn-tectonic magmatism in the Changle-Nan'ao Belt, South China. J. Geophys. Res. Solid Earth 128 (2). e2022JB025973.
Wolf, M.B., Wyllie, P.J., 1994. Dehydration-melting of amphibolite at 10 kbar: the effects of temperature and time. Contrib. Miner. Petrol. 115, 369–383.
Wones, D.R., 1989. Significance of the assemblage titanite+ magnetite+ quartz in granitic rocks. Am. Mineral 74 (7–8), 744–749.
Wong, J., Sun, M., Xing, G., Li, X.H., Zhao, G., Wong, K., Yuan, C., Xia, X.P., Li, L.M., Wu, F.Y., 2009. Geochemical and zircon U-Pb and Hf isotopic study of the Baijuhuajian metaluminous A-type granite: extension at 125–100 Ma and its tectonic significance for South China. Lithos 112 (3–4), 289–305.
Wong, J., Sun, M., Xing, G., Li, X.H., Zhao, G., Wong, K., Wu, F., 2011. Zircon U-Pb and Hf isotopic study of Mesozoic felsic rocks from eastern Zhejiang, South China: geochemical contrast between the Yangtze and Cathaysia blocks. Gondwana Res. 19 (1), 244–259.
Wu, F.Y., Yang, Y.H., Xie, L.W., Yang, J.H., Xu, P., 2006. Hf isotopic compositions of the standard zircons and baddeleyites used in U-Pb geochronology. Chem. Geol. 234, 105–126.
Xia, Y., Xu, X.S., Zhao, G.C., Liu, L., 2015. Neoproterozoic active continental margin of the Cathaysia block: Evidence from geochronology, geochemistry, and Nd–Hf isotopes of igneous complexes. Precambrian Res 269, 195–216.
Xie, C.F., Zhu, J.C., Zhao, Z.J., Ding, S.J., Fu, T.A., Li, Z.H., Zhang, Y.M., Xu, D.M., 2005. Zircon SHRIM P U-Pb age dating of garnet-acmite syenite: constraints on the Hercynian- Indosinian tectonic evolution of Hainan Island. Geol. J. China Universit. 11, 47–57. in Chinese with English abstract.

Xie, C.F., Zhu, J.C., Ding, S.J., Zhang, Y.M., Fu, T.A., Li, Z.H., 2006. Identification of Hercynian shoshonitic intrusive rocks in central Hainan Island and its geotectonic implications. Chin. Sci. Bull 51, 2507–2519. in Chinese with English abstract.
Xing, G.F., Chen, R., Yang, Z.L., Zhou, Y.Z., Li, L.M., Yang, J., Chen, Z.L., 2009. Characteristics and tectonic setting of Late Cretaceous volcanic magmatism in the coastal Southeast China. Acta Petrol. Sin. 25 (1), 77–91. in Chinese with English abstract.
Xu, D.R., Wu, C.J., Hu, G.C., Chen, M.L., Fu, Y.R., Wang, Z.L., Chen, H.Y., Hollings, P., 2016. Late Mesozoic molybdenum mineralization on Hainan Island, South China: Geochemistry, geochronology and geodynamic setting. Ore Geol. Rev 72, 402–433.
Xu, C.H., Zhang, L., Shi, H.S., Brix, M.R., Huhma, H.M., Chen, L.H., Zhang, M.Q., Zhou, Z. Y., 2017. Tracing an Early Jurassic magmatic arc from South to East China Seas. Tectonics 36, 466–492.
Xu, F., Zhang, G., Yan, W., Zhang, J., Yao, J., 2022. Subduction of the paleo-Pacific plate recorded by arc volcanism in the South China Sea margin. Gondwana Res. 110, 58–72.
Xu, X.S., Zhao, K., He, Z.Y., Liu, L., Hong, W.T., 2020. Cretaceous volcanic-plutonic magmatism in SE China and a genetic model. Lithos 402, 105728.
Yan, Q.S., Shi, X.F., Liu, J.L., Wang, K.S., Bu, W.R., 2010. Petrology and geochemistry of Mesozoic granitic rocks from the Nansha micro-block, the South China Sea: Constraints on the basement nature. J. Asian Earth Sci. 37, 130–139.
Yan, Q.S., Shi, X.F., Castillo, P.R., 2014. The late Mesozoic-Cenozoic tectonic evolution of the South China Sea: A petrologic perspective. J. Asian Earth Sci. 85, 178–201.
Yan, Q.S., Metcalfe, I., Shi, X.F., 2017. U-Pb isotope geochronology and geochemistry of granites from Hainan Island (northern South China Sea margin): Constraints on late Paleozoic-Mesozoic tectonic evolution. Gondwana Res. 49, 333–349.
Yan, Y., Yao, D., Tian, Z., Huang, C., Chen, W., Santosh, M., Yumul Jr, G.P., Dimalanta, C.B., Li, Z., 2018. Zircon U-Pb chronology and Hf isotope from the Palawan-Mindoro Block, Philippines: Implication to provenance and tectonic evolution of the South China Sea. Tectonics 37, 1063–1076.
Yang, Y.H., Wu, F.Y., Xie, L.W., Yang, J.H., Zhang, Y.B., 2011. High-precision direct determination of the $^{87}Sr/^{86}Sr$ isotope ratio of bottled Sr-rich natural mineral drinking water using multiple collector inductively coupled plasma mass spectrometry. Spectrochim. Acta, Part B 66, 656–660.
Yao, W.H., Li, Z.X., Li, W.X., Li, X.H., 2017. Proterozoic tectonics of Hainan Island in supercontinent cycles: New insights from geochronological and isotopic results. Precambrian Res 290, 86–100.
Yokoyama, K., Tsutsumi, Y., Kase, T., Queaño, K.L., Aguilar, Y.M., 2012. Provenance Study of Jurassic to Early Cretaceous sandstones from the Palawan microcontinental block. Philippines: Mem. Natl. Mus. Nat. Sci Tokyo 48, 177–199.
Yui, T.F., Heaman, L., Lan, C.Y., 1996. U-Pb and Sr isotopic studies on granitoids from Taiwan and Chinmen-Lieyii and tectonic implications. Tectonophysics 263 (1–4), 61–76.
Yumul Jr., G.P., 2007. Westward younging disposition of Philippine ophiolites and its implication for arc evolution. Isl Arc 16 (2), 306–317.
Zahirovic, S., Seton, M., Müller, R.D., 2014. The Cretaceous and Cenozoic tectonic evolution of Southeast Asia. Solid Earth 5 (1), 227–273.
Zhang, B., Guo, F., Zhang, X., Wu, Y., Wang, G., Zhao, L., 2019. Early Cretaceous subduction of Paleo-Pacific Ocean in the coastal region of SE China: petrological and geochemical constraints from the mafic intrusions. Lithos 334, 8–24.
Zhao, G.C., Cawood, P.A., 2012. Precambrian geology of China. Precambrian Res 222, 13–54.
Zhao, J.L., Qiu, J.S., Liu, L., Wang, R.Q., 2015. Geochronological, geochemical and Nd–Hf isotopic constraints on the petrogenesis of Late Cretaceous A-type granites from the southeastern coast of Fujian Province, South China. J Asian Earth Sci 105, 338–359.
Zhao, L.L., Wang, L., Tian, M.Z., Wu, F.D., 2017. Geochemistry and zircon U-Pb geochronology of the rhyolitic tuff on Port Island, Hong Kong: Implications for early Cretaceous tectonic setting. Geosci. Front 8, 565–581.
Zhao, X.L., Yu, S.Y., Jiang, Y., Mao, J.R., Yu, M.G., Chen, Z.H., Xing, G.F., 2019. Petrogenesis of two stages of Cretaceous granites in southwest Fujian Province: Implications for the tectonic transition of South-east China. Geol. J 54, 221–244.
Zhou, J.C., Chen, H.M., 2001. Geochemistry of late Mesozoic interaction between crust and mantle in southeastern Fujian Province. Geochimica 30 (6), 547–558 (in Chinese with English abstract).
Zhou, D., Sun, P., Jiang, S.J., Liu, X., Wang, Q., 2023. Geochronology and geochemistry of Early Cretaceous high-silica granites in the Nan'ao Island, South China: Petrogenesis and implications for lithospheric extension. J. Asian Earth Sci. 245, 105558.
Zhou, X.M., Li, W.X., 2000. Origin of Late Mesozoic igneous rocks in Southeastern China: implications for lithosphere subduction and underplating of mafic magmas. Tectonophysics 326, 269–287.
Zhou, Y., Liang, X.Q., Kröner, A., Cai, Y.F., Shao, T., Wen, S., Jiang, Y., Fu, J., Wang, C., Dong, C., 2015. Late Cretaceous lithospheric extension in SE China: constraints from volcanic rocks in Hainan Island. Lithos 232, 100–110.
Zhou, X.M., Sun, T., Shen, W., Shu, L., Niu, Y., 2006. Petrogenesis of Mesozoic granitoids and volcanic rocks in South China: A response to tectonic evolution. Episodes 29, 26–33.
Zhou, H.M., Xiao, L., Dong, Y.X., Wang, C.Z., Wang, F.Z., Ni, P., 2009. Geochemical and geochronological study of the Sanshui basin bimodal volcanic rock suite, China: Implications for basin dynamics in southeastern China. J Asian Earth Sci 34 (2), 178–189.
Zhu, K.Y., Li, Z.X., Xu, X.S., Wilde, S.A., 2014. A Mesozoic Andean-type orogenic cycle in southeastern China as recorded by granitoid evolution. Am J Sci. 314 (1), 187–234.
Zhu, B.Q., Wang, H.F., Chen, Y.W., Chang, X.Y., Hu, Y.G., Xie, J., 2004. Geochronological and geochemical constraint on the Cenozoic extension of Cathaysian lithosphere and tectonic evolution of the border sea basins in East Asia. J Asian Earth Sci. 24 (2), 163–175.